Spring 5-2020

Development of a High-throughput Platform for the Determination of Antiviral Therapeutics

Mason A. Crocker
University of Maine, mason.crocker@maine.edu

DEVELOPMENT OF A HIGH-THROUGHPUT PLATFORM FOR THE DETERMINATION OF ANTIVIRAL THERAPEUTICS

By

Mason Crocker

B.S. University of Maine, 2018

A THESIS

Submitted in Partial Fulfillment of the

Requirements for the Degree of

Master of Science

(In Microbiology)

The Graduate School

The University of Maine

May 2020

Advisory Committee:

Melissa Maginnis, Assistant Professor of Microbiology, Advisor

Sally Molloy, Assistant Professor of Genomics

Robert Gundersen, Associate Professor and Chair of Molecular and Biomedical Sciences

DEVELOPMENT OF A HIGH-THROUGHPUT PLATFORM FOR THE DETERMINATION OF ANTIVIRAL THERAPEUTICS

By Mason Crocker

Thesis Advisor: Dr. Melissa Maginnis

An Abstract of the Thesis Presented
in Partial Fulfillment of the Requirements for the
Degree of Master of Science
(in Microbiology)
May 2020

JC polyomavirus (JCPyV) persists in up to 90% of the global human population. In healthy individuals, the virus resides within the kidneys resulting in a low-level infection. However, in severely immunocompromised individuals, the virus can migrate to the central nervous system (CNS), causing the demyelinating disease progressive multifocal leukoencephalopathy (PML). Currently, this debilitating disease has no clinical therapeutic options and is almost universally fatal. Specifics of the JCPyV infectious cycle, as well as the limitations of traditional laboratory techniques, have previously hindered the search for antiviral agents with the potential to prevent or treat JCPyV infection. To this end, a new high-throughput, *in vitro* method to measure JCPyV infectivity, the In-cell Western (ICW) assay, has been adapted to allow for rapid, consistent, and impartial analysis of the antiviral properties of large libraries of drugs and other small compounds. Utilizing this ICW platform, a large-scale drug screen was performed using the National Institute for Health (NIH) Clinical Collection, a library of over 700 drugs and small compounds, to identify drugs and compounds that reduce JCPyV infectivity. Through analysis and characterization of these compounds, heretofore unknown therapeutic agents against

JCPyV have been identified, including drugs that target cell surface receptors and biochemical pathways involved in calcium and mitogen-activated protein (MAP) kinase signaling. These compounds are the focus of further characterization to identify the cell-based mechanism by which they inhibit JCPyV infection. Findings from this study provide new information that significantly advances the field in the development of antiviral compounds to treat or prevent PML.

ACKNOWLEDGEMENTS

My laboratory endeavors would have been in no way possible without the support, encouragement, and assistance of my fellow lab members; Sarah Nichols, Francesca Armstrong, Tristan Fong, Francois Levasseur, Remi Geohegan, Ashley Soucy, Colleen Mayberry, Kashif Mehmood, Michael Wilczek, Avery Bond, and Jeanne DuShane.

Collaborations with the Danthi laboratory (Indiana University) and the Mainou laboratory (Emory University) were absolutely essential to the research presented here.

This work was generously supported by funding from the National Institute of Allergy and Infectious Disease (NIAID) of the National Institutes of Health (NIH) under grant R15 AI144686 (MSM) and the Maine IDeA for Biomedical Research Excellence (ME-INBRE) Award (P20GM103423) from the National Institute of General Medical Sciences (NIGMS) from the NIH (MSM). Additionally, this work was supported in part by a Maine Space Grant Consortium Fellowship, Frederick H. Radke Undergraduate Research Fellowship, and a Degree-Related grant from the Graduate Student Government.

The instruction and guidance of Dr. Sally Molloy, Dr. Dorothy Croall, Dr. Robert Gundersen, and countless other professors of the Molecular and Biomedical Sciences department have helped to shape the student and scientist I have become.

The mentorship of Dr. Melissa Maginnis has presented me with the opportunities and means to grow as a student, a collaborator, and a professional, without which, the work presented here would not have been possible.

Thank you all.

TABLE OF CONTENTS

LIST OF TABLES

LIST OF FIGURES

Graphical Abstract

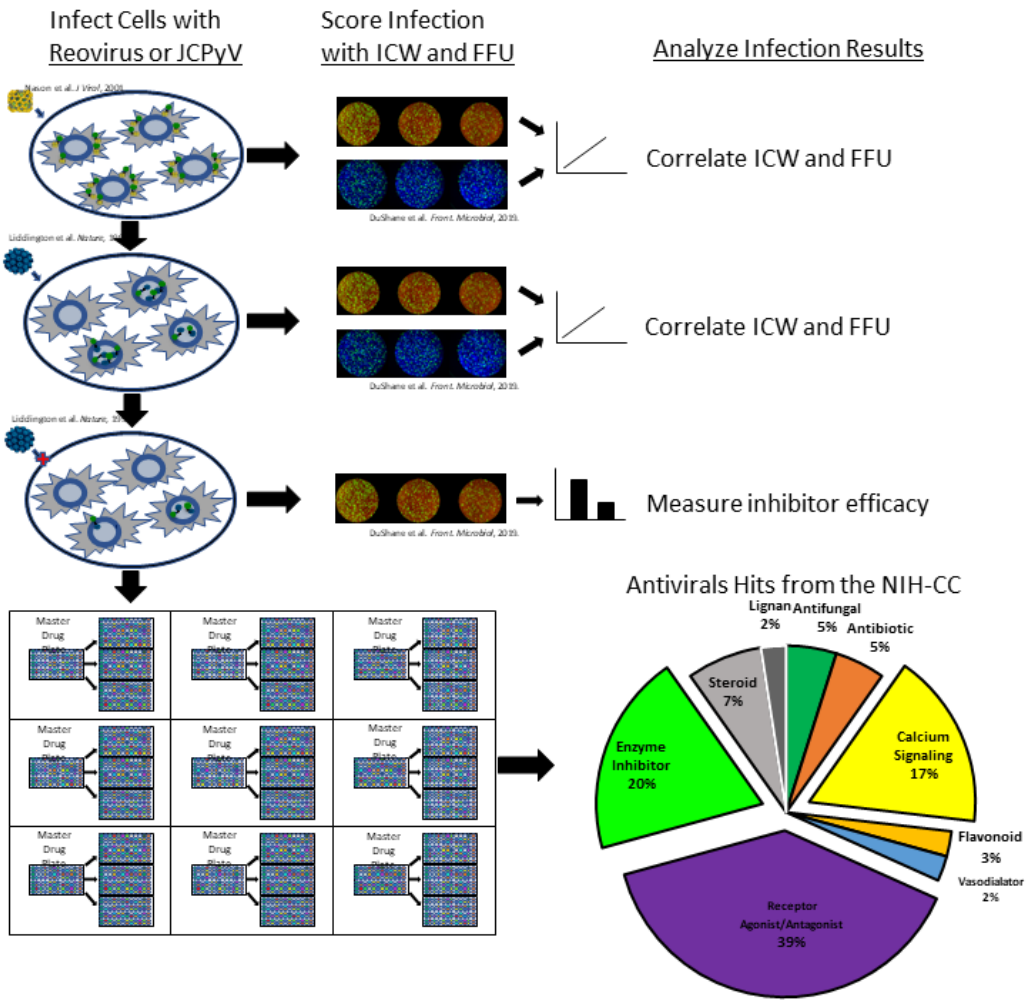

CHAPTER 1

INTRODUCTION

1.1. JC Polyomavirus Disease

Polyomaviridae is a large family of viruses that includes 14 species capable of infecting human hosts [1]. Infection by a number of these viruses is known to cause or contribute to human pathologies including different types of cancers, respiratory illnesses, diseases of the kidney and bladder, as well as a fatal, neurological condition known as progressive multifocal leukoencephalopathy (PML) [2]. PML is the result of neuron demyelination within the brain due to the lytic infection of oligodendrocytes. The destruction of these glial cells prevents proper nerve function and the subsequent formation of plaques within the brain (Figure 1), leading to the loss of cognitive, sensory, and motor functions as the disease progresses. Ultimately, this results in the afflicted individual's death, typically within a few months to one year of symptom onset [3]. Survival rates for patients suffering from PML have increased as the progression of the disease has become more understood and methods of early detection and effective highly active antiretroviral therapies (HAART) have been established [4]. However, survivability and the level of disability or impairment in these patients is based on a number of factors including age, degree of symptom onset, and general response to the treatment of the underlying immune compromise [5, 6].

The causative agent of this debilitating disease, JC polyomavirus (JCPyV), was first isolated in 1971 [7], 23 years after the first clinical description of PML, and has since been found to infect up to 90% of the global population [8]. The transmission of this virus is thought to occur via the peroral route during childhood and adolescence, with approximately 65% of the population infected by the age of 10 [9-11]. A key similarity among the human disease-causing polyomaviruses, including JCPyV, is that the initial infection, in healthy individuals, results in an asymptomatic infection that persists for the lifetime of the host [2, 12]. In the case of JCPyV, the site of this persistence is the kidney, where it is thought that healthy immune function ensures that the virus propagates at low levels without spreading to different tissues [13, 14].

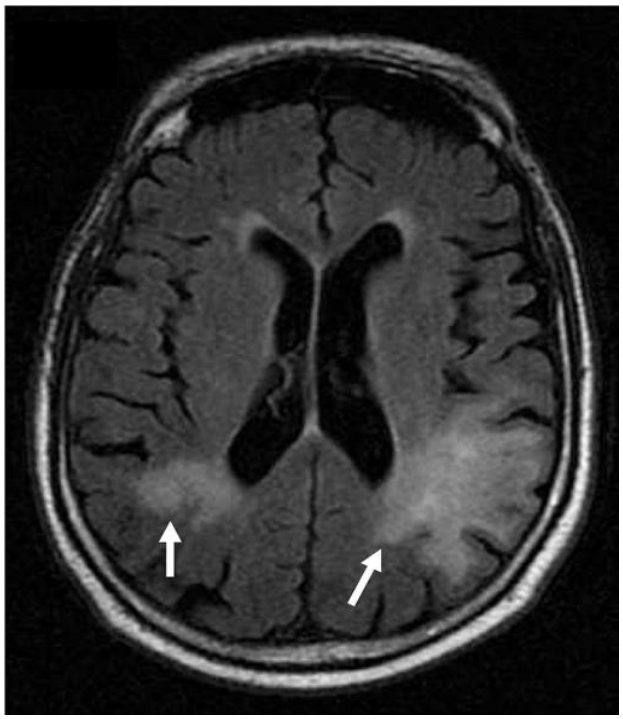

Figure 1. PML Pathogenesis. MRI of PML plaques (indicated by arrows) within the brain of a 70-year old patient. [15] (Figure adapted with permissions form Journal of NeuroVirology).

Upon severe immune system disruption, the virus is able to spread from the kidneys to the central nervous system (CNS) where it shifts from a persistent, asymptomatic infection to a highly lytic, pathogenic infection of oligodendrocytes and astrocytes. While the exact mechanism of this lifecycle shift is not fully understood, it appears that changes within a regulatory region of the viral genome is partially responsible [16-18]. In addition to cells of the kidney and CNS, other cells types have been proposed as essential for the viral migration and the development and progression of PML. B-cells have been suggested as a potential vehicle for JCPyV to cross the blood brain barrier (BBB) during such periods of immune suppression in a "Trojan horse" like model, in which JCPyV non-productively infects B-cells, gains entrance to the CNS via lymphocyte migration across the BBB, and then goes on to infect glial cells [19]. Additionally, research utilizing a humanized mice model suggests a specific and active role played by astrocytes in JCPyV infection of the brain. Astrocytes, which are readily infected by the virus, are also capable of supporting a highly productive infection, thereby giving the virus a

sort of 'jumping off point' within the CNS prior to oligodendrocyte infection, destruction, and neural demyelination [20].

The described migration of the virus from renal to glial sites of infection is seen most commonly in patients infected with the human immunodeficiency virus (HIV) or those undergoing prolonged immunomodulatory treatments for organ transplants, cancer, or any number of autoimmune diseases, most notably, multiple sclerosis (MS) patients treated with natalizumab, a monoclonal antibody against α4 integrins [3, 8, 21-23]. The onset of PML requires, at the very least, that JCPyV be able to access the CNS and that the host's immune response stays suppressed once this occurs. In the case of HIV infection, the HIV virions are able to enter the CNS inside infected monocytes that cross the BBB [24-26]. HIV replication within the CNS can then lead to disruption to the BBB, increasing its permeability [24, 25]. As immune suppression is a hallmark of HIV infection [27], this increased permeability at the BBB may set the stage for JCPyV to enter the CNS and begin the pathogenesis of PML. Similarly, in patients suffering from MS, the progression of their disease state can lead to a disrupted and more permeable BBB [28]. If these patients receive treatment with natalizumab, the neutralization of α4 integrins on leukocytes by the drug prevents their migration into the CNS [29, 30]. While this is the desired action of the drug, as overactive T leukocytes within the CNS leads to the pathology of multiple sclerosis [29, 30], it also results in reduced immune surveillance of the CNS [31]. Incidence of PML is approximately 4% in HIV patients and is an AIDS-defining illness [32]. The incidence of natalizumab-treated patients suffering from MS is 1:1000 to 1:100, although the incidence in this population is dependent on a number of factors, including the length of natalizumab treatment and a clinical history of other immunomodulatory therapies [33-35].

Unfortunately, at this time there are currently no specific clinical treatments for either PML or JCPyV infection [3] and the primary course of action is to attempt to rescue immune function, either through HAART treatment in HIV patients or to cease immunomodulatory therapies, such as that of natalizumab. However, these courses of action have the potential to induce immune reconstitution inflammatory syndrome (IRIS) [4, 36]. IRIS within the CNS can exacerbate PML pathology and can even be fatal in some cases [37]. Thus, gaining a better

understanding of the basic biology of the virus and virus-host cell interactions is an essential step in the search for effective antiviral therapies.

1.2. JCPyV Structure and Lifecycle

JCPyV is a nonenveloped virus with a proteinaceous capsid composed of three structural proteins, with viral protein 1 (VP1) being the major component. VP1 forms pentamers on the external surface of the capsid, and each VP1 pentamer interacts with either a VP2 or VP3 molecule on the internal face of the capsid [38, 39]. VP1 is also responsible for the interaction with host cell α2,6-linked lactoseries tetrasaccharide c (LSTc), which is required for viral attachment [40]. The viral double stranded DNA genome (Figure 2) is approximately 5.1 kb in length and contains the genes for viral products, the multifunctional large and small T antigens, expressed early during infection and the later expressed agnoprotein and structural proteins, VP1, VP2, and VP3 [3, 41]. Additionally, the genome contains a regulatory region with an origin of replication and appears to play a significant role in maintaining the persistent infection observed in the kidney. This region is also the site of a DNA rearrangement that appears to result in the viral lifecycle shift that allows JCPyV to migrate to the CNS as described above [17].

Following viral attachment to the host cell, JCPyV gains entry to the cell via clathrin-mediated endocytosis utilizing the serotonin receptor 5-hydroxytryptamine (5-HT) receptor, specifically the type 2 receptors (5-HT_2R), subtypes A, B, and C [42-44]. A schematic of JCPyV attachment, entry, and trafficking is depicted in Figure 3. The virus traffics through the endocytic compartment to the endoplasmic reticulum (ER) where it undergoes enzyme-mediated uncoating of the capsid [45]. The retrograde trafficking of JCPyV from the early endosome to the ER is accomplished by way of transfer to caveolin-1 vesicles in a Rab5-dependent manner [46]. This model for trafficking of JCPyV can be disrupted through the use of small molecule inhibitors, preventing the virus from establishing a productive infection. One

such inhibitor, Retro-2, forms a cyclic compound that interacts with yet undetermined host cell factors, preventing this trafficking pathway and stopping JCPyV infection from progressing [47].

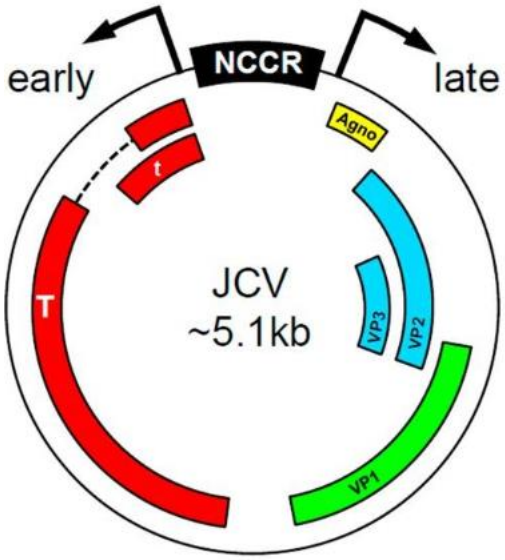

Figure 2. Schematic of JCPyV Genome. 'Early' genes on the left include large and small T antigen while 'Late' genes on the left include the 3 structural proteins, VP1, 2, and 3, as well as agnoprotein. Viral early and late genes are separated by a non-coding control region which contains the origin of replication and serves in a regulatory capacity [41]. (Figure adapted from PLoS One under Creative Commons licenses).

JCPyV then gains entry to the nucleus through nuclear localization signals revealed by uncoating. Following this, the early gene, large T antigen, is expressed through cellular transcription [3, 8]. T antigen regulates the host cell cycle via interaction with the tumor suppressor p53, driving the cell into S-phase for viral genome replication and expression of the late gene products that are required for viral capsid assembly [8]. The multi-functionality of viral T antigen allows it to coordinate and direct a number of steps required for late gene expression and direct control of the host cell cycle. T antigen is able to bind the regulatory region of the JCPyV genome, act as a helicase, and recruit host cell replication machinery (including polymerase) in order to drive viral genome replication. It also binds p53 and retinoblastoma (pRB) proteins, modulating their control of the cell cycle and usurping pRB recruitment of transcription factors to aid in the transcription and subsequent expression of viral late genes [23].

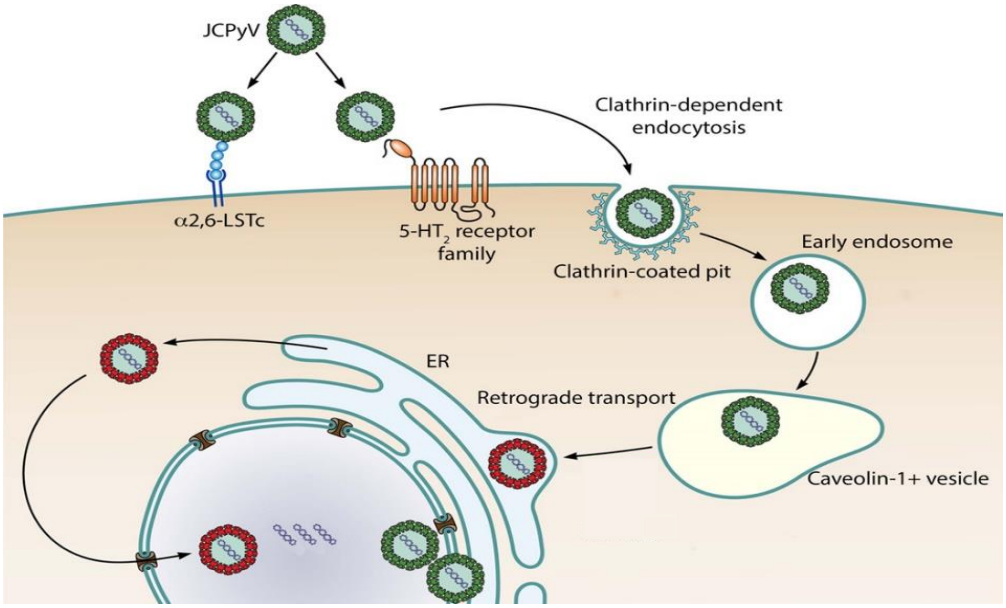

Figure 3. JCPyV Infectious Cycle. Viral attachment and entry requires both α2,6-LSTc and 5-HT_2R before proceeding through clathrin-mediated endocytosis. The virus then undergoes retrograde transport via a caveolin-1 vesicle to the ER, undergoing enzyme-mediated uncoating in the process. Once internalized the virus traffics to the nucleus for transcription and replication to occur [48] (Figure adapted with permissions form Journal of NeuroVirology).

1.3. Cellular Signaling Pathways in JCPyV Infection

Work published from the Maginnis lab in recent years has illustrated the role of the mitogen-activated protein (MAP) kinase cascade during JCPyV infection. In this model, JCPyV has been shown to activate MAP kinase signaling leading to phosphorylation of extracellular signal-regulated kinase (ERK) and subsequent phosphorylation of proteins needed for productive JCPyV infection as well as nuclear translocation of transcription factors thought to promote viral gene expression and replication [49, 50].

A number of chemical inhibitors of different kinases within this signaling cascade have been shown to inhibit productive JCPyV infection. These include PD98059 and U0126, inhibitors of MAP kinase kinase (MEK) 1 and 2, which prevent activation of the critical MAPK-ERK pathway and productive JCPyV infection [50]. Knockdown of an additional upstream activator of this

pathway, Rapidly Accelerated Fibrosarcoma kinase (RAF), has also been shown to prevent JCPyV infection [50]. BAY 43-9006, a drug that inhibits RAF [51], has similarly been shown to act as an inhibitor of JCPyV infection [52].

Currently unpublished work from the Maginnis lab has also suggested a critical role for calcium ion signaling in the infectious cycle of JCPyV. These experiments have illustrated a potential dependence by the virus on calcium signaling from the ER of an infected cell following endocytosis. Such calcium signaling is known to play a role in the lifecycle of other viruses during multiple steps of infection [53]. There is also evidence that a viral protein encoded by the JCPyV genome, agnoprotein, plays a role as a viroporin that increases the permeability of cellular membranes to calcium ions [54]. The preliminary model for the role of calcium is illustrated in Figure 4. In this model, JCPyV activation of the 5-HT_2R leads to activation of phospholipase C (PLC), subsequent cleavage of Phosphatidylinositol 4,5-bisphosphate (PIP2) to diacylglycerol (DAG) and inositol triphosphate (IP3). This leads to the activation of the IP3 receptor at the ER membrane and release of calcium ions into the cytosol, where it triggers a number of signaling mechanisms, including the translocation of Nuclear factor of activated T-cells (NFAT) to the nucleus as a result of activated calmodulin-dependent kinase [55]. Nuclear translocation of NFAT then drives the transcription of genes beneficial to the viral lifecycle [56]. While this exact signaling mechanism has not been definitively shown to occur during JCPyV infection, it is an area of on-going research.

Many aspects of JC polyomavirus infection, including gaps in our understanding of how the virus is reactivated during states of persistence and becomes pathogenic, are not fully understood [23, 57]. Combined with a lack of effective treatments for PML [3], the need for further research is evident. There are no tractable animal models of JCPyV infection and PML pathogenesis, and the development of animal models is in part limited due to the restricted viral host range, a limitation in the study of most polyomaviruses [2, 58]. Furthermore, rather than the disease progression seen in infected immunocompromised humans, JCPyV infection in animals leads to tumorigenesis due to production of large T antigen, an oncogene [59]. Although this may change in the future as work with a humanized mice model is explored [20, 60], this model is not currently widely used, nor is it without its own limitations and obstacles.

These limitations restrict research of JCPyV and PML pathogenesis to human cell culture models. JCPyV infection is only permissive in a limited number of tissues, specifically the kidneys and CNS, due to the requirement of JCPyV to interact with both α2,6-LSTc and 5-HT_2Rs for attachment and entry, further limiting how researchers can conduct experimental investigations of productive JCPyV infection [23, 43, 61].

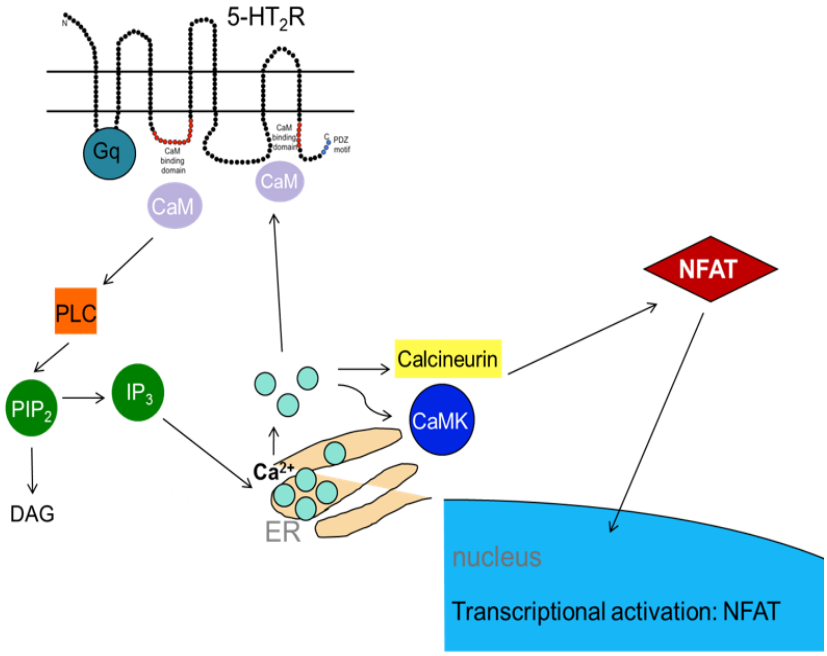

Figure 4. A Potential Role for Calcium Signaling in the JCPyV Infectious Lifecycle. Preliminary model for the activation of calcium release from the ER due to JCPyV activation of the 5-HT_2R and subsequent translocation of a transcriptional factor to the nucleus, spurring the expression of genes beneficial to the replication of the virus [62].

1.4. Experimental Methods of Viral Infectivity

Viral infectivity is typically quantified via assays such as the plaque forming assay and the focus forming unit (FFU) assay. The plaque assay relies on a virus infecting the cells of a monolayer and causing them to lyse, forming visible plaques that are easily quantified. Non-plaque forming viruses (such as JCPyV) cannot be analyzed using this method [63], leaving the FFU as one of the only reliable methods of quantifying JC polyomavirus infectivity [43]. The FFU procedure relies on indirect immunodetection staining and epifluorescence microscopy to visualize viral infectivity [39, 52]. Infected cells are stained using an antibody that recognizes a

viral protein, such as VP1 in the case of JCPyV. Cells are subsequently stained with a fluorescently-conjugated antibody. Fluorescence staining represents an infected cell, and the percentage of infected cells in a population can be quantified manually using an epifluorescence microscope. While this technique has been incredibly useful in JCPyV research, this method of measuring viral infectivity also presents several obstacles. The FFU introduces observer bias, relies on partial analysis of samples to generate representative data, and requires a large amount of time for data generation, reducing the productivity of JCPyV research and preventing high-throughput experimentation.

A relatively new technique, known as the In-cell Western assay (ICW), has been developed as a high-throughput method for visualizing protein expression within cells [64] and has been adapted by the field of virology for use in determining relative viral protein expression as a method of quantifying viral infectivity for influenza A and herpes simplex virus-1 [65, 66]. This high-throughput platform has also been used to successfully measure the effects of neutralizing antibodies, molecular inhibitors and antiviral molecules on the in vitro replication of Hantaan virus, as well as reovirus and rotavirus, and, more recently, JCPyV in the Maginnis lab [52, 65, 67, 68]. Moreover, the utility of the assay has been increased through its use in monitoring host protein expression as a result of viral infection [52, 69].

In contrast to the FFU, the ICW assay relies on indirect immunofluorescence detection via an automated infrared imaging system, the LI-COR Odyssey CLx. As with other indirect immunofluorescence detection techniques, cellular proteins are detected through the application of a protein-specific primary antibody and complementary secondary antibody conjugated to a fluorescent tag. The ICW technique employs the utilization of a near infrared (NIR) fluorescent secondary antibody, which allows for scanning of an entire sample plate via the LI-COR Odyssey CLx. The same sample preparation described for the FFU assay is used for this method of infectivity determination with the exception that the staining reagents used are conjugated to the NIR tags described, allowing for the use of an infrared imaging device. Because this device is automated, quantified data of viral infection is obtained much more rapidly than when measured via FFU. This saves, potentially, hours of data collection per experiment and allows for types of experimentation that are much larger in scope. This

functional advantage of the ICW, over the FFU, has the potential to greatly increase the rate of discovery in JCPyV research, particularly in the context of identifying antiviral agents for further development. A comparison of the FFU and ICW methods of quantifying viral infection is demonstrated in Figure 5. Although the use of this assay as an analytic tool across a number of different viral species is growing, the ICW requires validation before work with new viruses can begin.

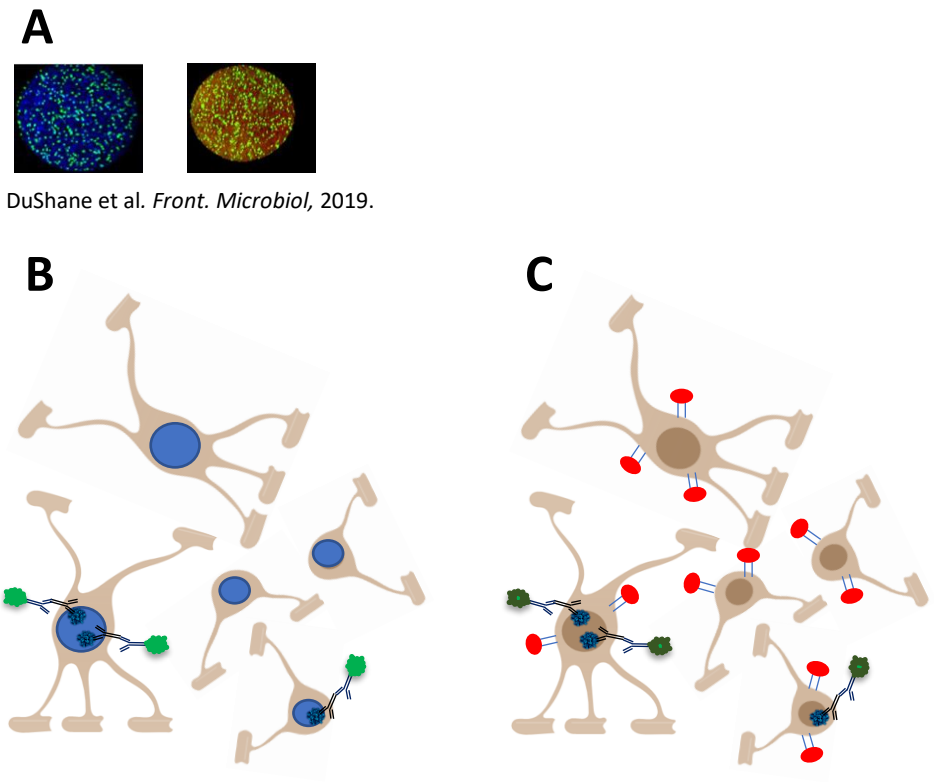

Figure 5. ICW vs FFU in Quantifying JCPyV Infection. A) SVG-A cells stained for FFU analysis (left) and SVG-A cells stained for ICW (right). B) Schematic of glial cells stained for FFU, nuclei have been stained with DAPI (blue). Immunostaining of JCPyV with green fluorescent antibody signals presence of VP1 expression within cellular nuclei. Performing a quotient of the number of VP1 positive nuclei and the number of DAPI stained nuclei yields a "percent infection." C) Schematic of glial cells stained for ICW, cell cytoplasm have been stained with nonspecific CellTag™ 700 (LI-COR) (red). Immunostaining of JCPyV with near infrared-green antibody signals presence of VP1 expression within cells. Performing a quotient of the near infrared intensity of the green signal and the near infrared intensity of the red signal yields a "percent response." (Images adapted from Frontiers in Microbiology under Creative Commons licenses, virion models adapted with permissions from Nature) (Created with BioRender).

1.5. Reovirus Background

In order to develop a novel ICW assay for measuring JCPyV infection, reovirus was selected as a model for the development of this assay with JCPyV-specific cell culture parameters. Reovirus is a nonenveloped dsRNA virus that infects many host species, including humans. While not typically implicated in human disease, it is a widely studied model of molecular virology and viral pathogenesis [70, 71]. The reovirus capsid has protruding filamentous proteins (σ1) that interact with host cell glycans and junctional adhesion molecule-A (JAM-A) to attach to the extracellular face of the cell. Reovirus is then thought to enter the host cell through interaction with β1 integrins [72]. Following entry, reovirus undergoes an enzyme-mediated uncoating process within lysosomes before being released into the cytosol where viral RNA dependent RNA polymerase, carried within the capsid, begins the transcription of the viral genome segments leading to viral replication and protein expression [73]. Figure 6 provides a general overview of the reovirus infectious lifecycle.

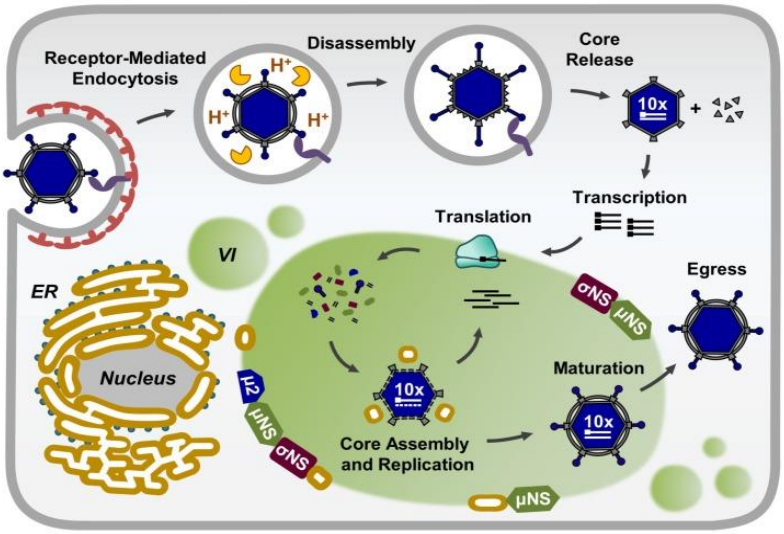

Figure 6. Reovirus Internalization. Reovirus capsid proteins adhere to host cells through interaction with cell surface sialic acid and JAM-A and gain entry to the cell via β1 integrins. Once uncoated the virus begins genome transcription and protein expression in the cytosol [70, 74]. (Figure adapted from Viruses under Creative Commons licenses).

CHAPTER 2

MATERIALS AND METHODS

2.1. Cell Culture

SVG-A cells, a mixed population of human fetal glial cells mainly composed of astrocytes [75], were maintained in Eagle's minimal essential medium (10% FBS, 1% penicillin/streptomycin, 0.2 % plasmocin) (c-MEM). Human embryonic kidney (HEK293A) cells (ATCC) expressing 5-HT_{2A}R were maintained in Dulbecco's modified Eagle's medium (10% FBS, 1% penicillin /streptomycin, 0.2% plasmocin) (c-DMEM) [43]. Cell lines were grown in a humidified incubator at 37°C with 5% CO_2. Cells were subcultured upon 90-100% confluency by passaging cells in fresh medium at a frequency of at least once every six days. Cell lines were kindly provided by Dr. Walter Atwood's laboratory (Brown University).

2.2. Reovirus Infectivity Assay

SVG-A and HEK293A cells were plated in 96-well plates (7,000 cells/well) and incubated at 37°C with 5% CO_2 until the cell monolayer reached ~70% confluency. Cells were infected with reovirus T1L strain inoculum (MOI indicated as per figure legend) in a total volume of 50 µL of complete media (lacking plasmocin) per well and incubated at 37°C for 1 h. Complete media was added back to appropriate wells (50 µL) and incubated at 37°C for 24 h. At 24 hours post infection (hpi), cells were fixed in 4% paraformaldehyde (PFA) at RT for 10 mins, washed once in sterile 1XPBS, and stored at 4°C until analysis.

2.3. JCPyV Infectivity Assay

SVG-A cells were plated in 96-well plates (7,000 cells/well) and incubated at 37°C until monolayer reached ~70% confluency. Cells were infected with JCPyV viral inoculum (MOI indicated per figure) in c-MEM (lacking plasmocin) in a total volume of 50 µL per well and incubated at 37°C for 1 h. Complete media (without plasmocin) was added back to appropriate wells (50 µL) and incubated at 37°C for 72 h. At 72 hpi, cells were fixed in 4% paraformaldehyde (PFA) at RT for 10 mins, washed once in sterile 1XPBS, and stored at 4°C until analysis.

2.4. Focus Forming Unit (FFU) Assay

2.4.1. Reovirus

Fixed cells were permeabilized in 1XPBS with 1.0% Triton X-100 at RT for 15 mins with gentle shaking. Cells were blocked with LI-COR Odyssey blocking buffer (TBS or PBS) at RT for 1.5 h with gentle rocking. Infected cells were stained with a rabbit derived T1L/T3D reovirus antisera (generously provided by Pranav Danthi, Indiana University) (1:5000) in LI-COR Odyssey TBS/PBS blocking buffer. Cells were incubated at 4°C O/N with gentle rocking. Samples were washed 3X with 0.1% Tween-TBS at RT for 10 mins with gentle rocking prior to being stained with a secondary antibody, anti-rabbit Alexa488 (Invitrogen [a11070]) (1:1000) in LI-COR Odyssey blocking buffer (TBS or PBS) at RT for 1 h with gentle rocking while protected from light. Cells were washed 3X with 0.1% Tween-TBS at RT for 10 mins with gentle rocking. Cell nuclei were stained with DAPI (1:1000) in 1XPBS at RT for 5 mins and then washed 3X with 0.1% Tween-TBS at RT for 10 mins with gentle rocking. Samples were analyzed via a Nikon Eclipse Ti epifluorescence microscope (Micro Video Instruments, Inc.) using Nikon NIS-Elements Basic Research software (version 4.5). Total cell counts were determined using a binary to identify DAPI-stained nuclei, and infected cell counts were determined manually in 5 fields of view, percent infection determined by a quotient of reovirus-positive cells and DAPI cells in each field of view and averaged for each well. Each viral MOI was analyzed in at least three wells. Samples were viewed at 10X magnification.

2.4.2. JCPyV

Fixed cells were permeabilized in 1XPBS with 1% Triton X-100 at RT for 15 mins with gentle shaking. Cells were blocked with LI-COR Odyssey blocking buffer (TBS or PBS) at RT for 1.5 h with gentle rocking. Infected cells were stained with a JCPyV VP1-specific antibody (Abcam [ab34756]) (1:1000) in LI-COR Odyssey TBS/PBS blocking buffer. Samples were incubated O/N at 4°C with gentle rocking then washed 3X with 0.1% Tween-TBS at RT for 10 mins with gentle rocking prior to being stained with a secondary antibody, Alexa488 (Invitrogen [a11017]) (1:1000) in LI-COR Odyssey blocking buffer (TBS or PBS) at RT for 1 h with gentle rocking while protected from light then washed 3X with 0.1% Tween-TBS at RT for 10 mins with

gentle rocking. Cell nuclei were stained with DAPI (1:1000) in 1XPBS at RT for 5 mins and washed 3X with 0.1% Tween-TBS at RT for 10 mins with gentle rocking. Samples were analyzed via epifluorescence microscopy. Total cell counts and infected cell counts were determined in 5 fields of view and averaged for each well, and percent infection was determined by a quotient of VP1-positive cells and DAPI-positive cells. Each viral MOI was analyzed in 3 wells. Samples were viewed at 20X magnification as described above.

2.5. In-Cell Western (ICW) Assay

Fixed cells were permeabilized in 1XPBS with 1.0% Triton X-100 at RT for 15 mins with gentle rocking. Cells were blocked with LI-COR Odyssey blocking buffer (TBS or PBS) at RT for 1.5 h with gentle rocking. Infected cells were stained with a rabbit derived T1L/T3D reovirus antisera (1:5000) in LI-COR Odyssey TBS/PBS blocking buffer or JCPyV VP1-specific antibody (Abcam [ab34756]) (1:1000) in LI-COR Odyssey TBS/PBS blocking buffer. Cells were incubated O/N at 4°C with gentle rocking. Samples were washed 3X with 0.1% Tween-TBS at RT for 10 mins with gentle rocking prior to being secondarily stained with a LI-COR antibody (680) conjugated with an IR fluorophore ([926-32210] (1:10,000)) in LI-COR Odyssey blocking buffer (TBS or PBS) and a LI-COR IR CellTag™ 700 ([926-41090] (1:500)) and incubated at RT for 1 h with gentle rocking. A sample of uninfected cells were treated with both antibodies and another sample was treated with only the secondary antibody as controls. Cells were washed 3X with 0.1% Tween-TBS at RT for 10 mins with gentle rocking. Samples were analyzed via the LI-COR Odyssey Automated IR Imager System with a focus offset of 3 mm and 700 and 800 nm channel intensities settings of 5 at a resolution of 84 μm. Percent ICW response was determined by a quotient of the intensity of the 800 channel and the intensity of the 700 channel.

2.6. Chemical Inhibitor Assay

SVG-A cells at 70% confluency were pretreated for 1 h (at 37°C with 5% CO2) with 50 μL of a molecular inhibitor prior to infection with JCPyV (MOI= 0.5 FFU/cell). Pretreatments were removed prior to infection. At 1 hpi, inhibitors were added back in the media feed. Of the four inhibitors used, PD98059 (2'-amino-3'-methoxyflavone), U0126 (1,4-diamino-2,3-dicyano-1,4-

bis[2-aminophenylthio] butadiene), and Retro-2 (2-{[(5-methyl-2-thienyl)methylene]amino}-*N*-phenylbenzamide) were present in the media for the full 72 h incubation period at 37°C. Bay43-9006 (4-(4-(3-(4-chloro-3-(trifluoromethyl)phenyl)ureido)phenoxy) N-methylpicolinamide 4-methylbenzenesulfonate), was also added back in the media but was removed at 2 hpi and replaced with untreated c-MEM for the full 72 h incubation period at 37°C. Each inhibitor used was compared to a vehicle control of DMSO. Experiment was analyzed via ICW.

2.7. NIH-CC Drug Screen

The National Institute of Health's Clinical Collection (NIH-CC) (kindly provided by the Mainou laboratory, Emory University), a library of 700 drugs and small molecules, was received frozen in solution with DMSO at a concentration of 1 mM. All drugs were stored in 96-well plates, with 80 drugs per plate across 9 plates. For each drug in the library, a 1:100 dilution was performed. Diluted drug samples (50 µL) were applied to SVG-A cells at 70% confluency for 1 h, 1 well per drug and incubated at 37°C. JCPyV (MOI= 0.5 FFU/cell, 30 µL) was added to every well while retaining the pretreated media in each well. At 1 hpi, 30 µL of c-MEM was added back to each well. Each experimental plate of 80 drugs also contained the controls: 4 wells of mock infected cells (receiving no virus), 4 wells of vehicle control DMSO for the drugs in the screen, 4 wells of PD98059 (50 µM) (positive control for viral inhibition), and 4 wells of vehicle control DMSO for the PD98059 control. Experiments were analyzed via ICW.

2.8. Validation of Topiramate

SVG-A cells at 70% confluency were pretreated for 1 h with various concentrations of topiramate at 37°C. This pretreatment was aspirated and the cells were infected for 1 h with JCPyV at a MOI of 1 (FFU/cell) at 37°C, in media containing topiramate at the same concentration as the pretreatment. Cells were fed with media containing topiramate and incubated at 37°C for 72 h fixed, stained for VP1, and processed for analysis by FFU. A vehicle control treated sample was included under the same conditions.

2.9. Statistical Methods

Statistical and computational analysis was conducted in Microsoft Excel. Statistical differences in both percent response and percent infection measurements were determined via the Student's t test. Z-score analysis of drugs from the NIH-CC was conducted as follows: an inhibitory effect against JCPyV for each drug in the screen was calculated by subtracting the percent ICW response of the negative control from the percent ICW response for each drug. The z-score of each inhibitory effect was calculated by subtracting the average inhibitory effect of all drugs within a single cell culture plate, divided by the standard deviation of the negative control for that plate, from the inhibitory effect of a given drug. Each z-score was compared to a 'hit' threshold that required it be lower than the negative value of the number of drugs on the same plate multiplied by the standard deviation inhibitory effect of those drugs. Statistical analysis performed in Microsoft Excel.

CHAPTER 3

RESULTS

3.1. Adaptation of the ICW for use in JCPyV Permissive Cell Models

The lack of a high-throughput platform for analysis of JCPyV infectivity has slowed research efforts and hampered the search for antiviral therapeutics for PML. The traditional FFU methodology for assessing viral infectivity is a reliable technique, albeit one that requires a large investment of time and person-hours to generate infectivity data. Adaptation of the newer ICW technique for use in JCPyV studies would provide researchers with an extremely high-throughput tool, allowing for larger scale experimentation. In contrast to the FFU assay, the ICW assay relies on indirect immunofluorescence detection via an automated infrared imaging system, the LI-COR Odyssey CLx. As with other indirect immunofluorescence detection techniques, cellular proteins are detected through the application of a protein-specific primary antibody and complementary secondary antibody conjugated to a fluorescent tag. The ICW technique employs the utilization of a near infrared (NIR) fluorescent secondary antibody, which allows for scanning of an entire sample plate via the LI-COR Odyssey CLx.

Published work by Iskarpatyoti et al. has shown that the ICW assay is a valid method of measuring relative differences in the *in vitro* infectivity of reovirus, a traditional model for laboratory analysis of viral pathogenesis [67, 71] in cell types pertinent to typical reovirus studies. In order to establish the ICW as a viable method for measuring JCPyV infection, we began by bridging the established use of the ICW with reovirus to viral infectivity studies in cell models permissive to JCPyV, SVG-A and HEK293A cells. To address this, the correlation between FFU and ICW determinations of reovirus infectivity in these cell types was investigated (Figure 7).

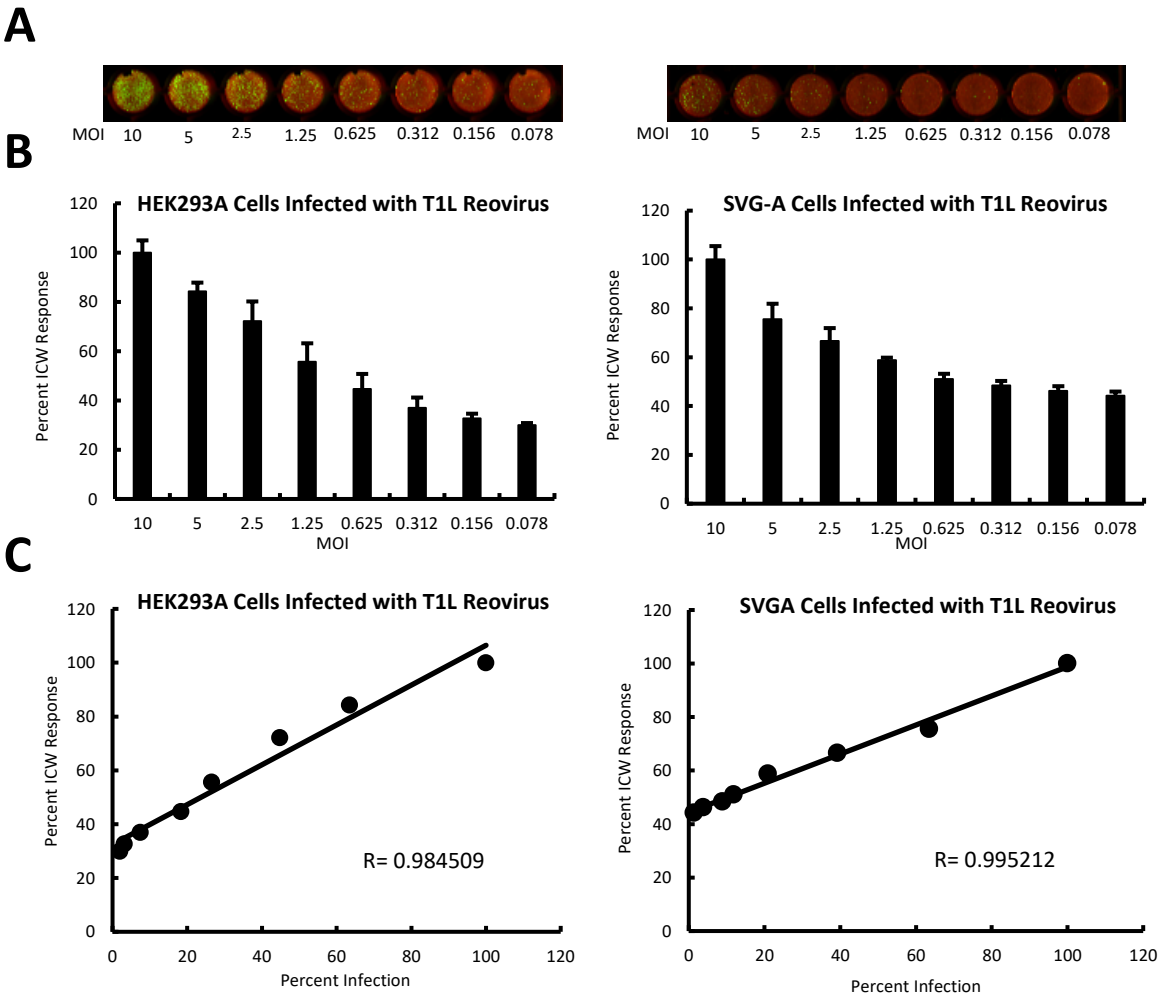

Figure 7. ICW Determination of Reovirus Infectivity. A) HEK293A (left) and SVG-A cells (right) infected with T1L strain reovirus at MOIs (FFU/cell) indicated were incubated for 24 h. Cells were then fixed and stained using ICW techniques and quantified via the automated LI-COR Odyssey CLx infrared imager. B) ICW infectivity data was collected at the viral MOIs indicated. Relative intensity values are expressed as percent response of the highest viral MOI used. Error bars represent SD from 3 replicates. C) Data from ICW experiments was compared to identical condition FFU infectivity assays. These samples were stained for viral protein expression and quantified as percent infection via epifluorescence microscopy. Microscopy data represents the average percentage of infected cells (total cell counts determined by DAPI staining) in five fields of view per well, performed in three replicates per viral MOI. Raw FFU data not shown. Linear correlation between assays was determined with a Pearson correlation coefficient test. Experiments shown are representatives of experiments performed in triplicate.

Both SVG-A and HEK293A cells were infected with reovirus at viral MOIs between 10 and 0.078 (FFU/cell), processed for ICW analysis, and imaged via the LI-COR Odyssey CLx (Figure 7A). The percent response to ICW analysis in both cell types was quantified and normalized to the highest level of reovirus infection (Figure 7B). The level of infection signified by this percent response was observed to correlate with viral MOI.

Comparison of this percent ICW response data to percent infection data from experiments completed in parallel, processed and imaged for FFU analysis, showed a high degree of correlation, as measured by Pearson correlation coefficients in both cell models approaching a value of 1 (Figure 7C). These experiments show that the ICW assay is useful for making relative determinations of reovirus infectivity in both SVG-A and HEK293A cell culture models.

3.2. The ICW Assay as a Method of Quantifying JCPyV Infection

Full validation of the ICW platform for adaptation to JCPyV studies required the first ever analysis of JCPyV infectivity with this new tool. To establish the viability of the ICW as a tool for measuring the infectivity of JCPyV *in vitro*, a similar investigation to that described above was completed to correlate the infectivity of JCPyV in SVG-A cells as determined by ICW and FFU methodologies. SVG-A cells were infected with JCPyV at viral MOIs between 2 and 0.0157 (FFU/cell), processed for ICW analysis, and imaged via the LI-COR Odyssey CLx. The percent response to ICW analysis was quantified and normalized to the highest level of JCPyV infection (Figure 8A). Comparison of this percent ICW response data to percent infection data from an experiment completed in parallel, processed and imaged for FFU analysis, showed a high degree of correlation, as measured by a Pearson correlation coefficient approaching a value of 1 (Figure 8B). Data are representative of independent experiments performed at varying MOIs [52].

ICW analysis of JCPyV in SVG-A cells demonstrates that the technique is a viable tool for assessing relative differences in viral infection. However, before this tool can be fully adapted for laboratory use in JCPyV studies, its utility in a functional assay must be examined.

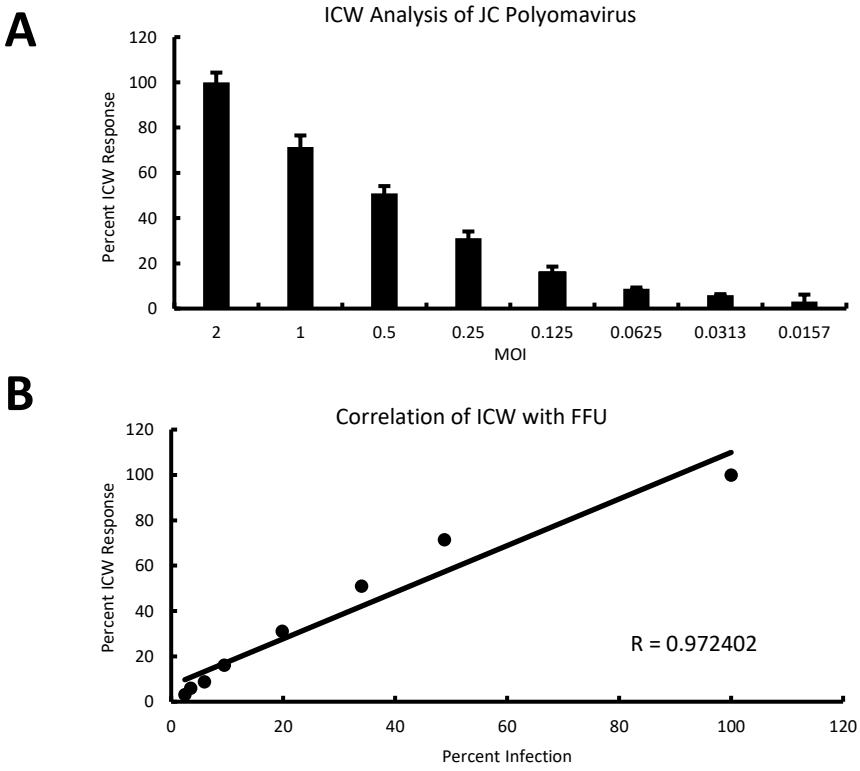

Figure 8: ICW Determination of JCPyV Infectivity. A) SVG-A cells infected with JCPyV at varying MOIs (FFU/cell) were incubated for 72 h. Cells were then fixed and stained for viral protein expression with an IR fluorescent dye before being quantified via the automated LI-COR Odyssey CLx infrared imager. Relative intensity values are expressed as percent response of the highest viral MOI used. Error bars represent SD from three replicates. B) Indirect immunofluorescence microscopy of samples infected under identical conditions was also performed. Microscopy data (not shown) represents the average percentage of infected cells in five fields of view (20X) per well, performed in triplicate per viral MOI. Linear correlation between assays was determined by a Pearson correlation test. Data are representative of independent experiments performed at varying MOIs [52].

3.3. Viral Inhibitor Efficacy as Assessed by ICW

The ICW was established as a method to perform large-scale screens to accelerate the pace of JCPyV research. Prior to performing the proposed drug screen with the NIH-CC, it was necessary to establish the utility of the ICW as an effective tool to test potential antivirals. To this end, SVG-A cells were treated with chemical inhibitors that were previously demonstrated to reduce JCPyV infection. Cells were pretreated with one of four chemical inhibitors (Figure 9),

then infected with JCPyV, and infection was measured by ICW analysis. For all inhibitors tested, a statistically significant reduction in JCPyV infection was observed via ICW analysis. Chemical inhibitors of MEK, PD98059 and U0126 [50], reduced JCPyV infection by approximately 54% and 35%, respectively, in comparison to the vehicle control for each chemical (Figure 9A and 9B). The other chemicals tested, Bay43-9006, an inhibitor of b-Raf [50], reduced JCPyV infectivity by approximately 62%, and Retro-2, an inhibitor of retrograde trafficking, reduced infectivity by approximately 27%, relative to the vehicle control (Figure 9C and 9D). These experiments, taken together, are a strong positive indicator that the ICW assay can be relied upon as an accurate tool in determining the relative level of JCPyV infection *in vitro* under various circumstances. This finding, in conjunction with the high-throughput capacity of the LI-COR Odyssey CLx, opens the door to large scale screening experiments that are currently infeasible given the time investment required to accomplish them by FFU analysis.

3.4. Large Scale Drug Screen of NIH-CC via ICW

Following the development of the ICW assay as a valid and effective tool for visualizing and quantifying relative difference in JCPyV infectivity in SVG-A cells [52], it was then adapted for the high-throughput utility of the assay in a large-scale drug screen. The NIH-CC was obtained through a collaboration with the Mainou laboratory (Emory University). This library contains 700 drugs and other small molecules (listed in full in Appendix A) that have been used in clinical trials in humans. This library was then screened against JCPyV and analyzed via ICW in three independent experiments. As described above, the effect of each of these 700 drugs and small compounds on the ability of JCPyV to infect SVG-A cells was then assessed as a z-score.

Of the 700 compounds assessed in these experiments, 42 were determined to meet the above described criteria to be considered as anti-JCPyV candidates under the conditions tested. As each plate was imaged independently via the LI-COR Odyssey CLx, the z-score threshold for each plate is independent of the others. The z-scores of every drug in each replicate were normalized to their respective z-score threshold and plotted in Figure 10A. In this normalization, any replicate with a z-score of less than −1 (Figure 10B) was considered to have crossed the threshold.

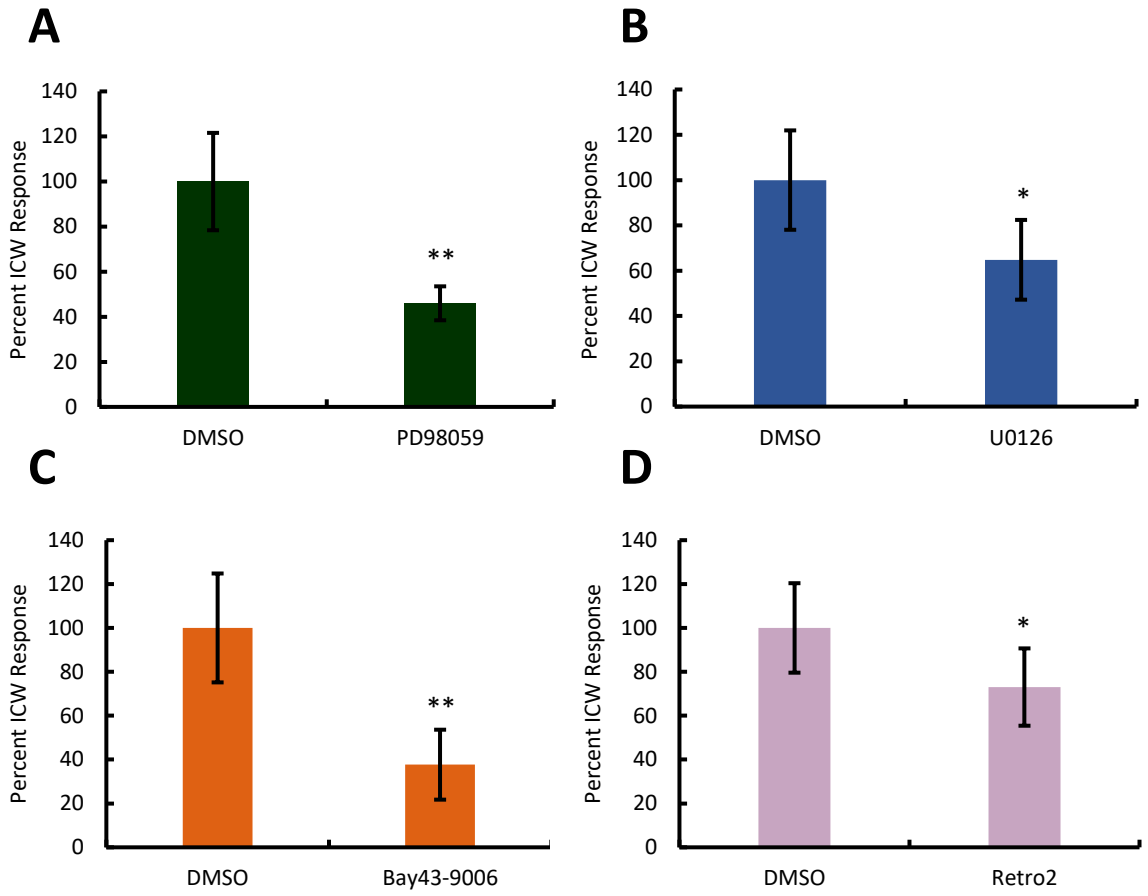

Figure 9. ICW Determination of Viral Inhibitor Efficacy. SVG-A cells were pre-treated with either the inhibitor indicated or a volume specific control of DMSO. Cells were then infected with JCPyV (MOI=0.5 FFU/cell) for 1 h. A) PD98059 (50 µM) an inhibitor of MEK. B) U0126 (10 µM) an inhibitor of MEK. C) Bay43-9006 (15 µM) an inhibitor of b-Raf. D) Retro-2 (100 µM) an inhibitor of retrograde trafficking. Following a 1 h infection, treated media was added back to wells; for PD98059, U0126, and Retro-2, the treated media remained on the cells for 72 h. For samples treated with media containing Bay43-9006, this media was removed 2 hpi and replaced with untreated media for the remainder of the 72 h. Cells were fixed and stained for viral protein expression with an IR fluorescent dye before being quantified via the automated LI-COR Odyssey CLx infrared imager (ICW). Error bars represent SD from six samples. *, $P<0.05$, **, $P<0.01$.

Compounds were determined to be an antiviral candidate if they crossed this z-score threshold in at least 2 of the 3 independent experiments. A literature review of the main mechanism of action, or function, of each of these candidate drugs returned a wide variety of results (Appendix B) and was used to group all 42 candidate drugs by function (Figure 10C).

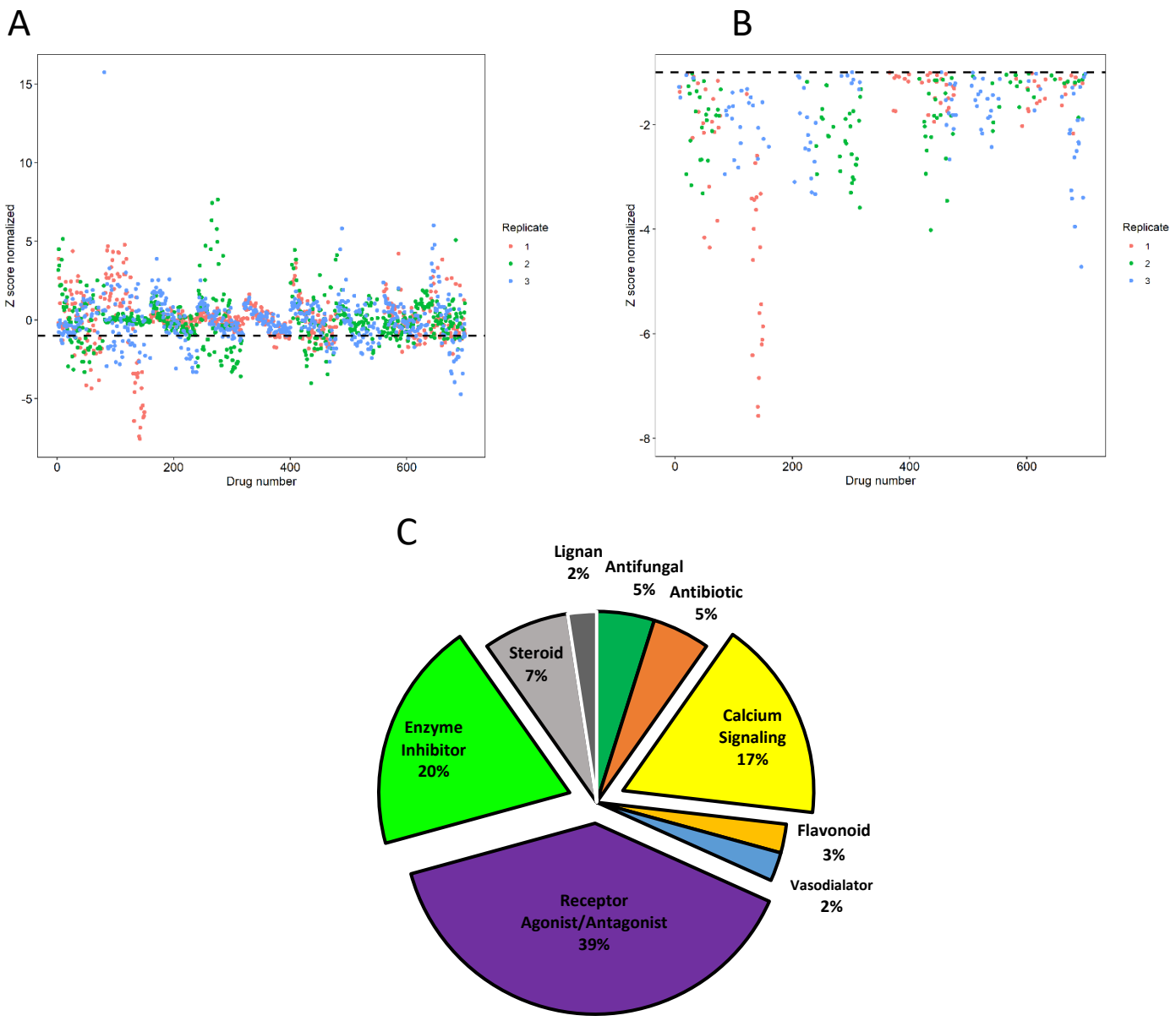

Figure 10. Identifying Antiviral Drugs from the NIH-CC. 700 individual drugs and small molecules were assessed for antiviral activity in a high-throughput screen against JCPyV in SVG-A cells. Cells were treated with media containing 10 µM concentrations of each drug or small molecule for 1 h then infected with JCPyV (MOI = 0.5 FFU/cell) for 1 h. Infected cells were then fed, incubated at 37˚C for 72 h, stained for VP1, and processed for ICW analysis. The statistical significance (z-score) of the effect of each drug on JCPyV infectivity was scored as described. z-scores were normalized to the z-score threshold

for the plate containing any particular drug. A) Plot of the normalized z-score of every drug in each replicate. B) All replicates with a normalized z-score that crossed the z-score threshold. Point color indicates which replicate each z-score belongs to; Orange represents replicate 1, Green represents replicate 2, Blue represents replicate 3. Drugs with z-scores crossing the normalized threshold of -1 in 2 of 3 replicates were considered candidate antivirals. C) Candidate drugs grouped by functionality.

3.5. Validating an Antiviral Compound

Having narrowed the library of 700 drugs and compounds down to 42 anti-JCPyV candidates, validation of the results of the drug screen in a targeted manner was then performed in order to identify anti-JCPyV candidates for further characterization. Topiramate, a drug sorted into the functional group containing inhibitors of calcium ion signaling (Appendix B), was applied to SVG-A cells at concentrations between 10 µM and 200 µM and tested against JCPyV infection at an MOI of 1 FFU/cell (Figure 11). In this experiment, concentrations of topiramate above 50 µM reduced JCPyV infectivity by approximately 30 to 40% when compared to the vehicle control. However, a dose response was not observed. The levels of JCPyV infection in cells treated with 50, 100, and 200 µM topiramate were not significantly different. The data shown here is representative of experiments performed in duplicate.

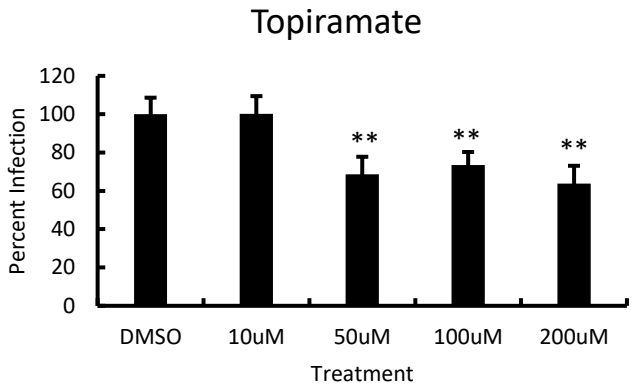

Figure 11. Effect of Topiramate on JCPyV Infection. SVG-A cells were treated for 1 h with the indicated concentration of the drug topiramate prior to infection with JCPyV at a MOI of 1 FFU/cell for 1 h. Infections were carried out in the presence of topiramate. Cells were then fixed at 72 hpi and stained for viral protein expression with a fluorescent tag before being quantified via FFU. Error bars represent SD from 3 samples. **, $P<0.05$.

CHAPTER 4

DISCUSSION AND FUTURE DIRECTIONS

Clinical treatment of PML is limited to attempts to rescue the underlying immune suppression that precipitated the disease onset, typically through the initiation of HAART treatment or the discontinuation of immunomodulatory therapies. However, these courses of action are not without their own risks, as reactivation of the immune system can result in induction of IRIS within the CNS [4, 36], with potentially disastrous or even fatal results [37]. While some antiviral therapies have been approved on a compassionate use basis, such as pembrolizumab [76], but these case-by-case treatments do not represent a realistic path forward for effective or scalable treatment development. The debilitating and often fatal outcomes associated with PML, paired with the lack of specific, approved clinical treatments, makes the identification and development of antiviral therapeutics a critical area of research. However, to date, laboratory research into the etiologic agent of this disease, JCPyV, has suffered from the lack of a high-throughput methodologies, hampering the progress of studies in this area. The lack of such tools was the catalyst for the work presented here. To this end, we have established the ICW assay as an effective tool for high-throughput JCPyV infectivity studies.

The experiments presented here, illustrate the utility of the ICW assay to make accurate determinations of relative differences in the infectivity of JCPyV in the SVG-A cell culture model, on par with traditional methodologies. We have expanded the use of this assay to visualize reductions in JCPyV infection due to chemical inhibitors of host cell processes usurped by the virus during productive infections. With these base requirements of laboratory utility and the capacity of this technique to reduce person-hours and overall time investment in the quantification of infectivity experiments by at least 8 hours per experiment, we have successfully adapted the ICW assay as a new high-throughput platform for JCPyV studies. It has not been previously feasible, without the use of highly-specialized equipment, to carry out this type of large-scale experimentation. The demonstrated potential of this assay to function in a

high-throughput capacity will greatly increase the rate of discovery in JCPyV research, aiding in the search for potential antiviral therapeutics, as well as that for other viral pathogens.

Our investigation of the high-throughput capability of this assay, the first large-scale screening of a drug library for antiviral agents against JCPyV analyzed by ICW, has yielded a wealth of interesting and suggestive results. These experiments have identified drugs and compounds with the potential to reduce JCPyV infectivity in vitro. While more work is necessary to validate these results, the identification of a number of drugs, whose mechanisms of action impact cellular pathways, known or expected to play critical roles in the JCPyV infectious cycle, reinforces confidence that these results may yet bear fruit in the search for therapeutics against JCPyV.

As many of the drugs within the NIH-CC library are currently FDA approved and on market, the possibility of observing antiviral activity against JCPyV by a drug already approved for clinical use was a distinct possibility. In fact, a previously performed drug screen of a different library of compounds by Brickelmaier et al. against JCPyV (in which a decidedly less high-throughput technique was employed) identified an on market antimalarial, mefloquine, as potentially having anti-JCPyV activity. In this work, they hypothesized this activity could be a result of the spatial similarity of mefloquine with nucleoside analogues, potentially allowing it to disrupt virus-specific genome replication via direct interaction with viral T antigen [77]. Mefloquine is a member of a drug class known as the quinoline-containing antimalarial drugs [78], and although the exact mechanism of action of mefloquine is not clear, other members of this drug class are more well studied. Their function may provide insight into that of mefloquine.

Perhaps the most well studied drug in this class, chloroquine, has been known for its immunomodulatory activity for some time. More recently, its potential antiviral properties have been an active area of research [79-82]. The primary mechanism of chloroquine is thought to be its activity as a base, raising the pH of endosomes and lysosomes considerably, disrupting their function. This activity modulates immune function by preventing the function of Toll-like receptors (TLR 7 and 9), reducing the production of cytokines and preventing nuclear

translocation of transcription factors that stimulate immune system associated genes [82]. The antiviral properties associated with chloroquine are likely a result, at least in part, of these activities but chloroquine and closely related analogues have also been shown to prevent HIV and dengue virus infectivity in vitro by altering the pH of endosomes containing progeny virus particles, preventing the proper formation and function of viral glycoproteins needed for subsequent host cell infections [79, 81]. Additionally, chloroquine has been shown to inhibit the ability of the hepatitis A virus to properly shed its capsid within acidic endosomes due to this change in pH [83]. Chloroquine and its closely related analogues have also been implicated as potential therapeutics for human coronaviruses [80] and are currently under investigation as potential therapies for SARS-CoV-2, the causative agent of COVID-19.

Unfortunately, clinical studies of mefloquine efficacy against JCPyV in PML patients has been inconclusive as of yet [84], however its use as an adjunct therapeutic has not been ruled out. The treatment of PML patients with mefloquine in conjunction with the drug mirtazapine, an antagonist of 5-HT_{2A}Rs, which are required for JCPyV entry, has been studied to some with some anecdotally positive clinical outcomes [85-87]. Although these case studies do not yet represent conclusive proof of clinical efficacy, the rapid adoption of mefloquine treatment for PML patients illustrates the great potential for high-throughput analysis to identify marketed drugs with anti-JCPyV activity that can be explored in a clinical capacity, relatively quickly.

Of the 42 anti-JCPyV candidates identified here by ICW analysis, sixteen are known agonists or antagonists of G-protein coupled receptors (GPCRs), several of which affect serotonin receptor signaling of the 5-HT_2R family utilized by JCPyV for host cell entry. Seven of these candidate drugs are known to impact the release, cellular retention, and signaling of calcium ions; processes known to impact the infectivity and lifecycle of many viruses, and for which preliminary research has indicated an important role in the JCPyV lifecycle. Additionally, 2 of the candidate drugs fall within the class of nonsteroidal anti-inflammatory drugs (NSAIDs), which have been previously suggested as a class of drugs capable of reducing JCPyV infection in vitro [77]. NSAIDs have been implicated as antiviral therapeutics previously with a mechanism similar to that offered by Bickelmaier et al., the selective inhibition of viral RNA synthesis of coronaviruses and influenza viruses [88, 89].

The GPCRs, 5-HT_2Rs are critical receptors for JCPyV entry into host cells [42-44]. Also of note, these receptors and chemical inhibitors of these receptors have been implicated in the infectious lifecycle of other viruses, including reovirus [90, 91]. The discovery of multiple 5-HTR targeting drugs via a screen of the NIH-CC against reovirus analyzed by ICW [90], implicated this class of receptors in the reovirus lifecycle and further analysis of one of these compounds, the agonist 5-nonyloxytryptamine (5-NT), found that its activity prevented the entry of chikungunya virus, mouse hepatitis virus, coronavirus, and reovirus into host cells [91]. Furthermore, a number of other viruses, including dangerous pathogens, HIV, Marburg virus, and ebolavirus, are known to use other GPCRs to gain entry into host cells [92]. Not only does the relevance of GPCRs in viral infections suggest the likelihood of these receptors as therapeutic targets of antivirals [92], but the findings of reovirus infectivity inhibition by 5-HTR targeting drugs through a high-throughput screening by ICW [90] and the implication of anti-JCPyV properties by many similar drugs in the experiments presented here, highlights the potential of the ICW platform in the discovery and characterization of new therapeutic agents.

Activation of the 5-HTRs is known to initiate cellular signaling pathways that result in the movement of calcium ions into the cytoplasm to act as secondary messengers [91]. Cellular signaling within cells via calcium ions is widespread and multifaceted and as such, has been implicated in numerous stages of viral lifecycles. The role of calcium in viral infections can be discussed in the context of direct viral association, membrane ion permeability, and calcium mediated signaling pathways [53]. The reliance of JCPyV on calcium ions in all three of these areas has been documented in the literature [54, 93] and explored in yet unpublished work from the Maginnis lab [62].The capsid of JCPyV is known to require calcium ions in order for proper viral uncoating at later stages of trafficking within host cells to occur [93]. A virally encoded protein, agnoprotein, has previously been shown to act as a viroporin, increasing the permeability at the plasma membrane of host cells to calcium ions in order to spur cell lysis and the release of viral progeny [54]. Finally, preliminary results have suggested a reliance on calcium ion release from the ER to the cytoplasm during JCPyV infection [62]. It is expected that this calcium release activates downstream effectors, namely calmodulin and calcineurin, to the benefit of the virus. In this working model, calcineurin activation of NFAT and calmodulin

stabilization of the 5-HTRs at the cellular membrane surface, help to drive viral replication and increase host cell susceptibility to infection [56, 62].

The many distinct roles suggested for calcium ions and the signaling events they mediate within JCPyV infected cells is of great interest in light of the results of the drug screen experiments presented here, as several candidate drugs effecting cell membrane calcium permeability in multiple ways were implicated. These included drugs that target cell surface calcium ion channels, as well as cell surface potassium channels, and ryanodine receptors (responsible for calcium movement across the membrane of the ER [94]). Despite these different targets, the actions of these drugs all appear to prevent movement of calcium ions into the cytoplasm, whether from the ER or the extracellular environment, where it can mediate the events JCPyV has apparently evolved to usurp this function for viral infection. The identification of the antiviral effects of these drugs by ICW, in addition to their potential role in therapeutic development, could present researchers with new compounds to help investigate and elucidate the importance of currently scrutinized cellular pathways in the infectious viral lifecycle.

The overlap of candidate drug function with JCPyV related cellular pathways was of particular importance in prioritizing drug candidates for validation in order to increase the chance of initial success in recapitulating the observed antiviral effect from the drug screen. Given the pathology of PML within the CNS, we also reasoned that potential therapeutics must be able to cross the BBB if they were to be viable clinical options. This rationale was consistent with a previous screening of drugs against JCPyV [77]. To this end, the candidate drug topiramate was selected for validation. Topiramate is an anticonvulsant and antimigraine drug known to inhibit multiple signaling pathways, including that of calcium ions via ion channel blockage. This particular mechanism and it activity within the CNS contributed to its selection for further validation [95]. Interestingly, topiramate is prescribed in some cases of PML in which plaque formation has resulted in seizures [96].

Although initial validation attempts did not show a dose-dependent decrease in JCPyV infection in cells treated with topiramate at concentrations as high as 200 μM, a statistically

significant reduction in infection of approximately 35% was observed (Figure 11). While further characterization and optimization of assays for the potential anti-JCPyV activity of topiramate are necessary, it is possible that increased concentrations of the drug may further reduce viral infection, resulting in both a dose response and more biologically significant results.

While the remainder of the candidate drugs may have functionalities not implicated in JCPyV infection, it is possible these drug functions could shine light on host cell pathways not currently understood to impact the ability of JCPyV to carry out a productive infections. This possibility is strengthened by what appears to be trends in the results, namely, the reduced infectivity observed in the presence of multiple drugs of related function. In the experiments conducted here, this trend was seen in cases of multiple inhibitors of histamine receptors (3), as well as drugs known to impact estrogen signaling (at least two) reducing JCPyV infection in a statistically significant manner. Both of these classes of drugs have demonstrated antiviral activity against influenza viruses [97, 98]. While it is impossible to say without additional validation of these results that these drugs and their documented mechanisms of action are indeed effective at reducing the ability of JCPyV to carry out a productive infection, it is certainly plausible. Such identification of previously unknown critical host cell pathways and machinery would add an additional facet to the potential research utility of the ICW assay in JCPyV research, an exciting prospect given the wide diversity of mechanisms and functionalities of this study's candidate antiviral compounds.

The use of a large-scale drug screens to identify previously unrecognized cellular pathways as key players in viral infection is an active area in the field of virology. Previous work published by a collaborator in this project, Dr. Bernardo Mainou, identified a key role played by microtubules and dynein 1, as well as the 5-HTR class of receptors, in reovirus infection of HeLa S3 cells when screening that virus against the same drug library (the NIH-CC) used in this study, using the same ICW platform [90, 91]. This precedent and the above rationale are suggestive that further analysis and characterization of the candidate drugs whose mechanisms of action do not appear to target known JCPyV related cellular functions, is warranted. The drug screen serves as a starting point to identify potential compounds that inhibit infection and

characterization of these compounds may reveal interesting, novel information about virus-host cell interactions and thus improves our understanding of the viral infectious cycle.

Of the 658 drugs and compounds that did not meet the criteria to be considered candidate antiviral agents, 75 were unable to be fully analyzed. This stems from the fact that, in the assay conditions performed, these drugs reduced the cellular content of samples significantly, indicating toxicity. This is an important reminder that in any high-throughput experimentation, the resulting data represents only a snapshot image of the whole story. Since it was only feasible to test one set of conditions across the drug screen, there is little doubt that compounds with significant antiviral activity were missed, as the optimal assay conditions of drugs across the library are certain to differ widely. This would imply that the remaining "non-candidate" drugs should warrant re-examination under varied circumstances, decreasing the treatment concentration of these 75 apparently toxic drugs, while increasing the treatment concentration of the non-toxic, non-candidates. Still, this re-assessment of the NIH-CC is well within reach of the ICW platform. Moreover, this assay will also allow for screens of any number of libraries or collections of drugs and compounds. The experimentation made accessible to researchers by the ICW, and its expanding use in the field of virology, makes the ICW an invaluable tool in the search for antivirals against JCPyV and other viral pathogens.

The ICW offers some important benefits as a tool in laboratory research of JCPyV and other viruses. Chief among these benefits is the high-throughput nature of an assay that fully automates the process of gathering viral infectivity data, freeing the efforts of researchers and increasing the rate of data acquisition, and hopefully, the rate of antiviral therapeutic development. Moreover, automated data acquisition removes all observer bias from the results of experiments, helping to reduce any doubt in experimental reproducibility. In addition, the process by which the LI-COR Odyssey CLx completes full field scanning of samples provides data from an entire sample population rather than representative sections of a population, producing results that are a more complete picture. The assay is not without its limitations though. Infectivity data produced through this method does not actually make determinations of cellular infectivity, it only provides data on the relative amounts of protein present in a sample. When assayed for a viral protein products, this method can provide insight into relative

infectivity changes, but not absolute changes. This means that the ICW requires preliminary experimentation and user familiarization prior to its use in new applications, as well as result validation to ensure the efficacy of results. Taken together, the ICW represents a new tool in the repertoire of virologist that provides experimental possibilities that were not easily adaptable to traditional methodologies but it is best viewed as augmenting these methods, not replacing them.

REFERENCES

1] Prado JCM, Monezi TA, Amorim AT, Lino V, Paladino A, Boccardo E. Human polyomaviruses and cancer: an overview. Clinics (Sao Paulo, Brazil). 2018;73:e558s.

[2] Jiang M, Abend JR, Johnson SF, Imperiale MJ. The role of polyomaviruses in human disease. Virology. 2009;384:266-73.

[3] Ferenczy MW, Marshall LJ, Nelson CD, Atwood WJ, Nath A, Khalili K, et al. Molecular biology, epidemiology, and pathogenesis of progressive multifocal leukoencephalopathy, the JC virus-induced demyelinating disease of the human brain. Clinical microbiology reviews. 2012;25:471-506.

[4] Sidhu N, McCutchan JA. Unmasking of PML by HAART: unusual clinical features and the role of IRIS. Journal of neuroimmunology. 2010;219:100-4.

[5] Dong-Si T, Richman S, Wattjes MP, Wenten M, Gheuens S, Philip J, et al. Outcome and survival of asymptomatic PML in natalizumab-treated MS patients. Annals of clinical and translational neurology. 2014;1:755-64.

[6] Dong-Si T, Gheuens S, Gangadharan A, Wenten M, Philip J, McIninch J, et al. Predictors of survival and functional outcomes in natalizumab-associated progressive multifocal leukoencephalopathy. Journal of neurovirology. 2015;21:637-44.

[7] Padgett BL, Walker DL, ZuRhein GM, Eckroade RJ, Dessel BH. Cultivation of papova-like virus from human brain with progressive multifocal leucoencephalopathy. Lancet (London, England). 1971;1:1257-60.

[8] Bellizzi A, Anzivino E, Rodio DM, Palamara AT, Nencioni L, Pietropaolo V. New insights on human polyomavirus JC and pathogenesis of progressive multifocal leukoencephalopathy. Clinical & developmental immunology. 2013;2013:839719.

[9] Taguchi F, Kajioka J, Miyamura T. Prevalence rate and age of acquisition of antibodies against JC virus and BK virus in human sera. Microbiology and immunology. 1982;26:1057-64.

[10] Bofill-Mas S, Formiga-Cruz M, Clemente-Casares P, Calafell F, Girones R. Potential transmission of human polyomaviruses through the gastrointestinal tract after exposure to virions or viral DNA. Journal of virology. 2001;75:10290-9.

[11] Elia F, Villani S, Ambrogi F, Signorini L, Dallari S, Binda S, et al. JC virus infection is acquired very early in life: evidence from a longitudinal serological study. Journal of neurovirology. 2017;23:99-105.

[12] Hara K, Sugimoto C, Kitamura T, Aoki N, Taguchi F, Yogo Y. Archetype JC virus efficiently replicates in COS-7 cells, simian cells constitutively expressing simian virus 40 T antigen. Journal of virology. 1998;72:5335-42.

[13] Monaco MC, Atwood WJ, Gravell M, Tornatore CS, Major EO. JC virus infection of hematopoietic progenitor cells, primary B lymphocytes, and tonsillar stromal cells: implications for viral latency. Journal of virology. 1996;70:7004-12.

[14] Wollebo HS, White MK, Gordon J, Berger JR, Khalili K. Persistence and pathogenesis of the neurotropic polyomavirus JC. Annals of neurology. 2015;77:560-70.

[15] Marzocchetti A, Wuthrich C, Tan CS, Tompkins T, Bernal-Cano F, Bhargava P, et al. Rearrangement of the JC virus regulatory region sequence in the bone marrow of a patient with rheumatoid arthritis and progressive multifocal leukoencephalopathy. Journal of neurovirology. 2008;14:455-8.

[16] Mischitelli M, Fioriti D, Videtta M, Degener AM, Antinori A, Cinque P, et al. Investigation on the role of cell transcriptional factor Sp1 and HIV-1 TAT protein in PML onset or development. Journal of cellular physiology. 2005;204:913-8.

[17] Saribas AS, Ozdemir A, Lam C, Safak M. JC virus-induced Progressive Multifocal Leukoencephalopathy. Future virology. 2010;5:313-23.

[18] Taoufik Y, de Goer de Herve MG. Editorial: Immune Control of JC Virus Infection and Immune Failure during Progressive Multifocal Leukoencephalopathy. Frontiers in immunology. 2017;8:1646.

[19] Chapagain ML, Nerurkar VR. Human polyomavirus JC (JCV) infection of human B lymphocytes: a possible mechanism for JCV transmigration across the blood-brain barrier. The Journal of infectious diseases. 2010;202:184-91.

[20] Kondo Y, Windrem MS, Zou L, Chandler-Militello D, Schanz SJ, Auvergne RM, et al. Human glial chimeric mice reveal astrocytic dependence of JC virus infection. The Journal of clinical investigation. 2014;124:5323-36.

[21] Langer-Gould A, Atlas SW, Green AJ, Bollen AW, Pelletier D. Progressive multifocal leukoencephalopathy in a patient treated with natalizumab. The New England journal of medicine. 2005;353:375-81.

[22] Tan CS, Koralnik IJ. Progressive multifocal leukoencephalopathy and other disorders caused by JC virus: clinical features and pathogenesis. The Lancet Neurology. 2010;9:425-37.

[23] Hirsch HH, Kardas P, Kranz D, Leboeuf C. The human JC polyomavirus (JCPyV): virological background and clinical implications. APMIS : acta pathologica, microbiologica, et immunologica Scandinavica. 2013;121:685-727.

[24] Toborek M, Lee YW, Pu H, Malecki A, Flora G, Garrido R, et al. HIV-Tat protein induces oxidative and inflammatory pathways in brain endothelium. Journal of neurochemistry. 2003;84:169-79.

[25] Mahajan SD, Aalinkeel R, Sykes DE, Reynolds JL, Bindukumar B, Fernandez SF, et al. Tight junction regulation by morphine and HIV-1 tat modulates blood-brain barrier permeability. Journal of clinical immunology. 2008;28:528-41.

[26] Williams DW, Anastos K, Morgello S, Berman JW. JAM-A and ALCAM are therapeutic targets to inhibit diapedesis across the BBB of CD14+CD16+ monocytes in HIV-infected individuals. Journal of leukocyte biology. 2015;97:401-12.

[27] Schnittman SM, Greenhouse JJ, Psallidopoulos MC, Baseler M, Salzman NP, Fauci AS, et al. Increasing viral burden in CD4+ T cells from patients with human immunodeficiency virus (HIV) infection reflects rapidly progressive immunosuppression and clinical disease. Annals of internal medicine. 1990;113:438-43.

[28] Vos CM, Geurts JJ, Montagne L, van Haastert ES, Bö L, van der Valk P, et al. Blood-brain barrier alterations in both focal and diffuse abnormalities on postmortem MRI in multiple sclerosis. Neurobiology of disease. 2005;20:953-60.

[29] von Andrian UH, Engelhardt B. Alpha4 integrins as therapeutic targets in autoimmune disease. The New England journal of medicine. 2003;348:68-72.

[30] Singer BA. The role of natalizumab in the treatment of multiple sclerosis: benefits and risks. Therapeutic advances in neurological disorders. 2017;10:327-36.

[31] Berger JR, Houff S. Opportunistic infections and other risks with newer multiple sclerosis therapies. Annals of neurology. 2009;65:367-77.

[32] Berger JR. Progressive multifocal leukoencephalopathy in acquired immunodeficiency syndrome: explaining the high incidence and disproportionate frequency of the illness relative to other immunosuppressive conditions. Journal of neurovirology. 2003;9 Suppl 1:38-41.

[33] Bloomgren G, Richman S, Hotermans C, Subramanyam M, Goelz S, Natarajan A, et al. Risk of natalizumab-associated progressive multifocal leukoencephalopathy. The New England journal of medicine. 2012;366:1870-80.

[34] Calabrese LH, Molloy E, Berger J. Sorting out the risks in progressive multifocal leukoencephalopathy. Nature Reviews Rheumatology. 2015;11:119-23.

[35] Berger JR, Fox RJ. Reassessing the risk of natalizumab-associated PML. Journal of neurovirology. 2016;22:533-5.

[36] González-Suarez I, Rodríguez de Antonio L, Orviz A, Moreno-García S, Valle-Arcos MD, Matias-Guiu JA, et al. Catastrophic outcome of patients with a rebound after Natalizumab treatment discontinuation. Brain and behavior. 2017;7:e00671.

[37] Tan K, Roda R, Ostrow L, McArthur J, Nath A. PML-IRIS in patients with HIV infection: clinical manifestations and treatment with steroids. Neurology. 2009;72:1458-64.

[38] Chen XS, Stehle T, Harrison SC. Interaction of polyomavirus internal protein VP2 with the major capsid protein VP1 and implications for participation of VP2 in viral entry. The EMBO journal. 1998;17:3233-40.

[39] Stroh LJ, Maginnis MS, Blaum BS, Nelson CD, Neu U, Gee GV, et al. The Greater Affinity of JC Polyomavirus Capsid for alpha2,6-Linked Lactoseries Tetrasaccharide c than for Other Sialylated Glycans Is a Major Determinant of Infectivity. Journal of virology. 2015;89:6364-75.

[40] Neu U, Maginnis MS, Palma AS, Ströh LJ, Nelson CD, Feizi T, et al. Structure-function analysis of the human JC polyomavirus establishes the LSTc pentasaccharide as a functional receptor motif. Cell host & microbe. 2010;8:309-19.

[41] Wharton KA, Jr., Quigley C, Themeles M, Dunstan RW, Doyle K, Cahir-McFarland E, et al. JC Polyomavirus Abundance and Distribution in Progressive Multifocal Leukoencephalopathy (PML) Brain Tissue Implicates Myelin Sheath in Intracerebral Dissemination of Infection. PloS one. 2016;11:e0155897.

[42] Pho MT, Ashok A, Atwood WJ. JC virus enters human glial cells by clathrin-dependent receptor-mediated endocytosis. Journal of virology. 2000;74:2288-92.

[43] Assetta B, Maginnis MS, Gracia Ahufinger I, Haley SA, Gee GV, Nelson CD, et al. 5-HT2 receptors facilitate JC polyomavirus entry. Journal of virology. 2013;87:13490-8.

[44] Mayberry CL, Soucy AN, Lajoie CR, DuShane JK, Maginnis MS. JC Polyomavirus Entry by Clathrin-Mediated Endocytosis Is Driven by β-Arrestin. Journal of virology. 2019;93.

[45] Neu U, Stehle T, Atwood WJ. The Polyomaviridae: Contributions of virus structure to our understanding of virus receptors and infectious entry. Virology. 2009;384:389-99.

[46] Querbes W, O'Hara BA, Williams G, Atwood WJ. Invasion of host cells by JC virus identifies a novel role for caveolae in endosomal sorting of noncaveolar ligands. Journal of virology. 2006;80:9402-13.

[47] Nelson CD, Carney DW, Derdowski A, Lipovsky A, Gee GV, O'Hara B, et al. A retrograde trafficking inhibitor of ricin and Shiga-like toxins inhibits infection of cells by human and monkey polyomaviruses. mBio. 2013;4:e00729-13.

[48] Maginnis MS, Nelson CD, Atwood WJ. JC polyomavirus attachment, entry, and trafficking: unlocking the keys to a fatal infection. Journal of neurovirology. 2015;21:601-13.

[49] DuShane JK, Wilczek MP, Mayberry CL, Maginnis MS. ERK Is a Critical Regulator of JC Polyomavirus Infection. Journal of virology. 2018;92.

[50] DuShane JK, Mayberry CL, Wilczek MP, Nichols SL, Maginnis MS. JCPyV-Induced MAPK Signaling Activates Transcription Factors during Infection. International journal of molecular sciences. 2019;20.

[51] Adnane L, Trail PA, Taylor I, Wilhelm SM. Sorafenib (BAY 43-9006, Nexavar®), a Dual-Action Inhibitor That Targets RAF/MEK/ERK Pathway in Tumor Cells and Tyrosine Kinases VEGFR/PDGFR in Tumor Vasculature. Methods in Enzymology: Academic Press; 2006. p. 597-612.

[52] DuShane JK, Wilczek MP, Crocker MA, Maginnis MS. High-Throughput Characterization of Viral and Cellular Protein Expression Patterns During JC Polyomavirus Infection. Frontiers in microbiology. 2019;10:783.

[53] Zhou Y, Frey TK, Yang JJ. Viral calciomics: interplays between Ca2+ and virus. Cell calcium. 2009;46:1-17.

[54] Suzuki T, Orba Y, Okada Y, Sunden Y, Kimura T, Tanaka S, et al. The human polyoma JC virus agnoprotein acts as a viroporin. PLoS pathogens. 2010;6:e1000801.

[55] Berridge MJ. Inositol trisphosphate and calcium signalling mechanisms. Biochimica et biophysica acta. 2009;1793:933-40.

[56] Manley K, O'Hara B A, Gee GV, Simkevich CP, Sedivy JM, Atwood WJ. NFAT4 is required for JC virus infection of glial cells. Journal of virology. 2006;80:12079-85.

[57] Tan CS, Ellis LC, Wuthrich C, Ngo L, Broge TA, Jr., Saint-Aubyn J, et al. JC virus latency in the brain and extraneural organs of patients with and without progressive multifocal leukoencephalopathy. Journal of virology. 2010;84:9200-9.

[58] Frost EL, Lukacher AE. The importance of mouse models to define immunovirologic determinants of progressive multifocal leukoencephalopathy. Frontiers in immunology. 2014;5:646.

[59] Maginnis MS, Atwood WJ. JC virus: an oncogenic virus in animals and humans? Seminars in cancer biology. 2009;19:261-9.

[60] Tan CS, Broge TA, Jr., Seung E, Vrbanac V, Viscidi R, Gordon J, et al. Detection of JC virus-specific immune responses in a novel humanized mouse model. PloS one. 2013;8:e64313.

[61] Marshall LJ, Major EO. Molecular regulation of JC virus tropism: insights into potential therapeutic targets for progressive multifocal leukoencephalopathy. Journal of neuroimmune pharmacology : the official journal of the Society on NeuroImmune Pharmacology. 2010;5:404-17.

[62] Soucy AN. Defining the Role of IP3R-Medicated ER Calcium Flux in JC Polyomavirus Infection. Digital Commons: University of Maine; 2018.

[63] Baer A, Kehn-Hall K. Viral concentration determination through plaque assays: using traditional and novel overlay systems. Journal of visualized experiments : JoVE. 2014:e52065.

[64] Aguilar HN, Zielnik B, Tracey CN, Mitchell BF. Quantification of rapid Myosin regulatory light chain phosphorylation using high-throughput in-cell Western assays: comparison to Western immunoblots. PloS one. 2010;5:e9965.

[65] Wan Y, Zhou Z, Yang Y, Wang J, Hung T. Application of an In-Cell Western assay for measurement of influenza A virus replication. Journal of virological methods. 2010;169:359-64.

[66] Fabiani M, Limongi D, Palamara AT, De Chiara G, Marcocci ME. A Novel Method to Titrate Herpes Simplex Virus-1 (HSV-1) Using Laser-Based Scanning of Near-Infrared Fluorophores Conjugated Antibodies. Frontiers in microbiology. 2017;8:1085.

[67] Iskarpatyoti JA, Willis JZ, Guan J, Morse EA, Ikizler M, Wetzel JD, et al. A rapid, automated approach for quantitation of rotavirus and reovirus infectivity. Journal of virological methods. 2012;184:1-7.

[68] Ma HW, Ye W, Chen HS, Nie TJ, Cheng LF, Zhang L, et al. In-Cell Western Assays to Evaluate Hantaan Virus Replication as a Novel Approach to Screen Antiviral Molecules and Detect Neutralizing Antibody Titers. Frontiers in cellular and infection microbiology. 2017;7:269.

[69] Cuartas-López AM, Hernández-Cuellar CE, Gallego-Gómez JC. Disentangling the role of PI3K/Akt, Rho GTPase and the actin cytoskeleton on dengue virus infection. Virus research. 2018;256:153-65.

[70] Danthi P, Holm GH, Stehle T, Dermody TS. Reovirus receptors, cell entry, and proapoptotic signaling. Advances in experimental medicine and biology. 2013;790:42-71.

[71] Ezzati P, Komher K, Severini G, Coombs KM. Comparative proteomic analyses demonstrate enhanced interferon and STAT-1 activation in reovirus T3D-infected HeLa cells. Frontiers in cellular and infection microbiology. 2015;5:30.

[72] Maginnis MS, Forrest JC, Kopecky-Bromberg SA, Dickeson SK, Santoro SA, Zutter MM, et al. Beta1 integrin mediates internalization of mammalian reovirus. Journal of virology. 2006;80:2760-70.

[73] Joklik WK. Virus synthesis and replication: reovirus vs. vaccinia virus. The Yale journal of biology and medicine. 1980;53:27-39.

[74] Tenorio R, Fernández de Castro I, Knowlton JJ, Zamora PF, Sutherland DM, Risco C, et al. Function, Architecture, and Biogenesis of Reovirus Replication Neoorganelles. Viruses. 2019;11.

[75] Major EO, Miller AE, Mourrain P, Traub RG, de Widt E, Sever J. Establishment of a line of human fetal glial cells that supports JC virus multiplication. Proceedings of the National Academy of Sciences of the United States of America. 1985;82:1257-61.

[76] Cortese I, Muranski P, Enose-Akahata Y, Ha S-K, Smith B, Monaco M, et al. Pembrolizumab Treatment for Progressive Multifocal Leukoencephalopathy. New England Journal of Medicine. 2019;380:1597-605.

[77] Brickelmaier M, Lugovskoy A, Kartikeyan R, Reviriego-Mendoza MM, Allaire N, Simon K, et al. Identification and Characterization of Mefloquine Efficacy against JC Virus In Vitro. Antimicrobial Agents and Chemotherapy. 2009;53:1840-9.

[78] Baudry S, Pham YT, Baune B, Vidrequin S, Crevoisier C, Gimenez F, et al. Stereoselective passage of mefloquine through the blood-brain barrier in the rat. The Journal of pharmacy and pharmacology. 1997;49:1086-90.

[79] Savarino A, Boelaert JR, Cassone A, Majori G, Cauda R. Effects of chloroquine on viral infections: an old drug against today's diseases? The Lancet Infectious diseases. 2003;3:722-7.

[80] Vincent MJ, Bergeron E, Benjannet S, Erickson BR, Rollin PE, Ksiazek TG, et al. Chloroquine is a potent inhibitor of SARS coronavirus infection and spread. Virology Journal. 2005;2:69.

[81] Wang LF, Lin YS, Huang NC, Yu CY, Tsai WL, Chen JJ, et al. Hydroxychloroquine-inhibited dengue virus is associated with host defense machinery. Journal of interferon & cytokine research : the official journal of the International Society for Interferon and Cytokine Research. 2015;35:143-56.

[82] Schrezenmeier E, Dörner T. Mechanisms of action of hydroxychloroquine and chloroquine: implications for rheumatology. Nature Reviews Rheumatology. 2020;16:155-66.

[83] Devaux CA, Rolain JM, Colson P, Raoult D. New insights on the antiviral effects of chloroquine against coronavirus: what to expect for COVID-19? International journal of antimicrobial agents. 2020:105938.

[84] Clifford DB, Nath A, Cinque P, Brew BJ, Zivadinov R, Gorelik L, et al. A study of mefloquine treatment for progressive multifocal leukoencephalopathy: results and exploration of predictors of PML outcomes. Journal of neurovirology. 2013;19:351-8.

[85] Schröder A, Lee D-H, Hellwig K, Lukas C, Linker RA, Gold R. Successful Management of Natalizumab-Associated Progressive Multifocal Leukoencephalopathy and Immune Reconstitution Syndrome in a Patient With Multiple Sclerosis. Archives of Neurology. 2010;67:1391-4.

[86] Moenster RP, Jett RA. Mirtazapine and mefloquine therapy for progressive multifocal leukoencephalopathy in a patient infected with human immunodeficiency virus. American Journal of Health-System Pharmacy. 2012;69:496-8.

[87] Kurmann R, Weisstanner C, Kardas P, Hirsch HH, Wiest R, Lämmle B, et al. Progressive multifocal leukoencephalopathy in common variable immunodeficiency: mitigated course under mirtazapine and mefloquine. Journal of neurovirology. 2015;21:694-701.

[88] Amici C, Di Caro A, Ciucci A, Chiappa L, Castilletti C, Martella V, et al. Indomethacin has a potent antiviral activity against SARS coronavirus. Antiviral therapy. 2006;11:1021-30.

[89] Glatthaar-Saalmüller B, Mair KH, Saalmüller A. Antiviral activity of aspirin against RNA viruses of the respiratory tract-an in vitro study. Influenza and other respiratory viruses. 2017;11:85-92.

[90] Mainou BA, Zamora PF, Ashbrook AW, Dorset DC, Kim KS, Dermody TS. Reovirus Cell Entry Requires Functional Microtubules. mBio. 2013;4:e00405-13.

[91] Mainou BA, Ashbrook AW, Smith EC, Dorset DC, Denison MR, Dermody TS. Serotonin Receptor Agonist 5-Nonyloxytryptamine Alters the Kinetics of Reovirus Cell Entry. Journal of virology. 2015;89:8701-12.

[92] Maginnis MS. Virus-Receptor Interactions: The Key to Cellular Invasion. Journal of molecular biology. 2018;430:2590-611.

[93] Nelson CD, Ströh LJ, Gee GV, O'Hara BA, Stehle T, Atwood WJ. Modulation of a pore in the capsid of JC polyomavirus reduces infectivity and prevents exposure of the minor capsid proteins. Journal of virology. 2015;89:3910-21.

[94] Hamilton S. Ryanodine receptors. Cell calcium. 2005;38:253-60.

[95] Naegel S, Obermann M. Topiramate in the prevention and treatment of migraine: efficacy, safety and patient preference. Neuropsychiatric disease and treatment. 2010;6:17-28.

[96] Lima MA, Bernal-Cano F, Clifford DB, Gandhi RT, Koralnik IJ. Clinical outcome of long-term survivors of progressive multifocal leukoencephalopathy. Journal of neurology, neurosurgery, and psychiatry. 2010;81:1288-91.

[97] Robinson DP, Hall OJ, Nilles TL, Bream JH, Klein SL. 17β-estradiol protects females against influenza by recruiting neutrophils and increasing virus-specific CD8 T cell responses in the lungs. Journal of virology. 2014;88:4711-20.

[98] Xu W, Xia S, Pu J, Wang Q, Li P, Lu L, et al. The Antihistamine Drugs Carbinoxamine Maleate and Chlorpheniramine Maleate Exhibit Potent Antiviral Activity Against a Broad Spectrum of Influenza Viruses. Frontiers in microbiology. 2018;9:2643.

APPENDIX A

Table A. Drugs Included in the NIH-CC

Daunorubicin hydrochloride	Cefixime trihydrate	SR 57227A
Meloxicam	Mecillinam	Dolasetron mesylate
Aminoglutethimide	Cladribine	Enalaprilat
Methazolamide	Docetaxel	Zolmitriptan
Priscoline hydrochloride	Cyproheptadine hydrochloride	Nitrazepam
Hydrocortisone	Rolipram	Oxymetholone
Doxycycline	Chlordiazepoxide	Telithromycin
Valproic acid	Corticosterone	Prednisolone sodium succinate
Nicardipine hydrochloride	Demeclocycline	Modafinil
Proxymetacaine	Clomifene citrate	SKF 83566 hydrobromide
Terbutaline sulfate	Tetracycline	Parecoxib sodium
Gatifloxacin	Sulfisoxazole	Stiripentol
Pyrazinamide	Ethynylestradiol	Sibutramine
Ethionamide	Levofloxacin	Vindesine sulfate
Lovastatin	4-Phenylbutyric acid	Palonosetron hydrochloride
Methocarbamol	Rabeprazole	Naproxen sodium
Clopidogrel	Naphazoline hydrochloride	Mepirizole
Phenoxybenzamine hydrochloride	Rutin	Methylandrostenediol
Loperamide hydrochloride	Edrophonium chloride	Tibolone
S(-)-Timolol maleate	Letrozole	Dichloroacetic acid
Penicillin V	Ethacrynic acid	Tryptoline
Flunisolide	Zucapsaicin	Diazepam
DL-Penicillamine	Aminolevulinic acid	Ornidazole
Minoxidil	Nortriptyline hydrochloride	Voriconazole
Orphenadrine hydrochloride	Moclobemide	Glycopyrronium bromide
Furosemide	Omeprazole	Pravastatin sodium
5-Fluorouracil	Taxifolin-(+/-)	Bestatin
Procyclidine hydrochloride	CCPA	PD 81723
Pyridostigmine bromide	Nitrendipine	Isradipine

Table A. Continued

Tolazamide	Repaglinide	Benactyzine hydrochloride
Metyrapone	Vincristine sulfate	Argatroban
Pindolol	Mestranol	Brucine
Probenecid	Crotamiton	Cefdinir
Fexofenadine hydrochloride	Flumazenil	Carmofur
Hydrochlorothiazide	Desoximetasone	Homoveratrylamine
Folic acid	Mevastatin	Artemether
Prednisone	Ebselen	Montelukast sodium
Penicillin G potassium	Naftopidil	Zalcitabine
Eryped	CGS 12066B dimaleate	Tacrolimus
Medrysone	Atracurium besylate	Tegafur
Methylprednisolone	Ursodeoxycholic acid	Itraconazole
Doxazosin	Estrone 3-sulfate sodium salt	Cefaclor
Azathioprine	Bicalutamide	Tocainide
Hydroxyzine pamoate	Halometasone monohydrate	Methyltestosterone
Cortisol 21-acetate	TFMPP hydrochloride	Beclomethasone
Mafenide acetate	Ozagrel hydrochloride	Nialamide
Medroxyprogesterone 17-acetate	Benidipine hydrochloride	Valdecoxib
Labetalol hydrochloride	Nefazodone hydrochloride	Raltitrexed
Triamcinolone acetonide	Sertraline hydrochloride	Ipidacrine
Thiabendazole	Indinavir sulfate	Pilocarpine hydrochloride
Prednisolone	Pioglitazone hydrochloride	Nicorandil
Ofloxacin	Epirubicin hydrochloride	Famciclovir
Prilocaine hydrochloride	Hexamethylenebisacetamide	Amiodarone hydrochloride
Nadolol	Moxifloxacin hydrochloride	Nizatidine
Felodipine	Venlafaxine hydrochloride	Topotecan hydrochloride
Carbidopa	AM 404	Salmeterol
Midodrine hydrochloride	Irinotecan hydrochloride	SDM25N hydrochloride
Nabumetone	Buflomedil hydrochloride	Calcipotriol
Tropicamide	Doxorubicin hydrochloride	Lacidipine
Propafenone	CGS 15943	Ketoconazole
Fluorometholone	Imatinib mesylate	Pergolide mesylate
Thiothixene	Perospirone hydrochloride	Dofetilide
Cetirizine	Milnacipran hydrochloride	L-694,247
Indomethacin hydrate	Rofecoxib	Nalidixic acid

Table A. Continued

Promethazine hydrochloride	Rosiglitazone maleate	Pazufloxacin
Fluoxetine hydrochloride	Nafadotride	Honokiol
Minocycline hydrochloride	Escitalopram oxalate	Maltol
19-Norethindrone acetate	Tropisetron hydrochloride	Levocetirizine
Altretamine	Fenoldopam mesylate	Etomidate
Ipratropium bromide	Tosufloxacin tosilate	Megestrol acetate
Fludarabine	Vardenafil citrate	GR 89696 fumarate
Rifapentine	Physostigmine hemisulfate	Lamotrigine
Hexachlorophene	Nornicotine	Rifaximin
Oxacillin sodium	Loxoprofen sodium	Irsogladine maleate
Acitretin	Tegaserod maleate	Lofexidine hydrochloride
Acyclovir	Trimebutine maleate	Benazepril hydrochloride
Betamethasone	Calcitriol	Nobiletin
Oxybutynin hydrochloride	Progesterone	Irbesartan
Diflunisal	Urapidil hydrochloride	Etomoxir
Nicotine	Betaxolol hydrochloride	Tripelennamine hydrochloride
Dexamethasone	5-Fluoro-2-pyrimidone	Synephrine
6-Azauridine	Mosapride citrate	Diclofenac sodium
Atomoxetine hydrochloride	1,1-Dimethyl-4-phenylpiperazinium iodide	Bupropion hydrochloride
Phenothiazine	Penciclovir	Cefpodoxime proxetil
Dipyridamole	Pizotyline maleate	Azelastine hydrochloride
6-Aminoindazole	Dexchlorpheniramine maleate	Meropenem
Enrofloxacin	Formoterol fumarate dihydrate	Vecuronium bromide
Idebenone	Cinanserin	Idarubicin hydrochloride
Tamoxifen	Ropivacaine hydrochloride	Tramadol hydrochloride
Azithromycin	Prochlorperazine maleate	Chlorpheniramine maleate
Eszopiclone	Pefloxacin mesylate	Naltrindole hydrochloride hydrate
Taxifolin-(+)	Terbinafine hydrochloride	Epigallocatechin gallate
GR 79236	Oxyphenonium bromide	Pramipexole
5-Nonyloxytryptamine hydrochloride	Hyperoside	Selegiline hydrochloride

Table A. Continued

Chloramphenicol	Haloperidol hydrochloride	2-Chloroadenosine
Ormetoprim	Lamivudine	Cilastatin sodium
Sulfacetamide	Alosetron monohydrochloride	Lorazepam
Phenprobamate	Loratadine	Phenelzine sulfate
Doxepin hydrochloride	Dextromethorphan hydrobromide, monohydrate	Prazosin hydrochloride hydrate
Rifabutin	Maprotiline hydrochloride	Amiloride hydrochloride hydrate
Atropine	Riluzole hydrochloride	Valaciclovir hydrochloride
11-Deoxycortisol	Pentoxifylline	Trazodone hydrochloride
Methotrexate trihydrate	Fluperlapine	R(+)-SCH-23390 hydrochloride
Clobenpropit	MK 886	Remacemide hydrochloride
Tranilast	Pancuronium dibromide	Sumatriptan succinate
Mesna	Cisapride hydrate	Tolterodine tartrate
Nafcillin sodium	Fluvoxamine maleate	Itavastatin calcium
Isoproterenol hydrochloride	Lansoprazole	Donepezil hydrochloride
Ketoprofen	DuP 697	Bifonazole
Propofol	Esmolol hydrochloride	Procarbazine hydrochloride
L-Thyroxine	Piribedil hydrochloride	Droperidol
Cortisone	Granisetron hydrochloride	Flecainide hydrochloride
7-Nitroindazole	Efavirenz	Diphenoxylate hydrochloride
Benproperine phosphate	Nelfinavir mesylate	Dextrorphan D-tartrate
Bumetanide	Ticlopidine hydrochloride	Anagrelide hydrochloride
SB 205607 dihydrobromide	Losartan potassium	Galanthamine hydrobromide
Levonorgestrel	(-)-Cotinine	Pemolide
Miglitol	Duloxetine hydrochloride	Lidocaine
Buspirone hydrochloride	Clotrimazole	Ritonavir
Raloxifene hydrochloride	Fluticasone propionate	Disulfiram
Methylprednisolone acetate	Itopride hydrochloride	Quetiapine fumarate
Troxipide	Moxonidine hydrochloride	Salbutamol sulfate

Table A. Continued

MDL 73005EF hydrochloride	Nifekalant hydrochloride	Bifemelane hydrochloride
Rufloxacin hydrochloride	Indatraline hydrochloride	Scopolamine hydrobromide
Benztropine mesylate	L-NMMA acetate	Nifedipine
Levosulpiride	Mestanolone	Tacrine hydrochloride
Nitazoxanide	Dactinomycin	Indirubin
Oxiconazole nitrate	Amlodipine	Oligomycin A
Clomipramine hydrochloride	Mirtazapine	Roxatidine acetate hydrochloride
Piperacillin sodium	Artesunate	Esomeprazole magnesium
Quinidine	Olopatadine hydrochloride	Trifluoperazine hydrochloride
Resveratrol	Altanserin hydrochloride	Glimepiride
Dehydroepiandrosterone	5-Methoxytryptamine	Cetraxate hydrochloride
Lomifylline	Cephalexin hydrate	Huperzine A
Secnidazole	Actarit	Metronidazole
Captopril	Linopirdine dihydrochloride	19-Nortestosterone
Dilantin	Cefatrizine propylene glycol	Beta-estradiol
Nicotinamide	Tremulacin	Ranolazine dihydrochloride
5-Azacytidine	Valsartan	Nalbuphine hydrochloride
Enalapril maleate	Zeranol	(+/-)-Vesamicol hydrochloride
Bethanechol chloride	Oxcarbazepine	E-4031 dihydrochloride
Secoisolariciresinol	Desloratadine	Cytarabine
Benzylimidazole	Amlexanox	Raclopride
Budesonide	Tadalafil	Paroxetine maleate
Zardaverine	Aripiprazole	Famotidine
Loxapine succinate	Citalopram hydrobromide	Dexbrompheniramine maleate
Propranolol hydrochloride	P1075	Ketotifen fumarate
Acarbose	Triptolide	Rimcazole dihydrochloride
Carbamazepine	Tinidazole	Goserelin acetate
Dantrolene sodium	Amisulpride	Spironolactone
Naloxone hydrochloride	Triclabendazole	Carbinoxamine maleate

Table A. Continued

Dehydrocholic acid	Olmesartan medoxomil	Meclizine hydrochloride
Piceid	Ketorolac tromethamine	Ganciclovir
Torasemide	Linezolid	Praziquantel
Prostaglandin E1	Otenzepad	Meclofenamic acid sodium salt
Nisoldipine	Didanosine	Memantine hydrochloride
Chlorambucil	Milrinone	(+)-cis-Diltiazem hydrochloride
Ampicillin sodium	Tiagabine hydrochloride	Chloroxine
Dapsone	Nevirapine	Estradiol valerate
Cyclophosphamide hydrate	Ifenprodil hemitartrate	Nitrofurantoin
Miconazole nitrate	Latanoprost	Cefazolin sodium
Phylloquinone	Azasetron hydrochloride	Chlorpromazine hydrochloride
Ondansetron	Bisoprolol fumarate	Isotretinoin
Mupirocin	Olanzapine	Warfarin sodium
Thioridazine hydrochloride	Picrotin - Picrotoxinin	Cimetidine
19-Norethindrone	Telmisartan	Gemfibrozil
Celecoxib	Ramipril	Dicyclomine hydrochloride
Floxuridine	Pterostilbene	Fluconazole
Indapamide	Cerivastatin sodium	Zolpidem tartrate
Imipramine hydrochloride	Ampiroxicam	Chlorothiazide
Quinapril hydrochloride	Xanthinol nicotinate	Flubendazole
Perphenazine	Lofepramine	Beclomethasone dipropionate
Norfloxacin	Clarithromycin	Testosterone
Spectinomycin	Benzbromarone	Homoharringtonine
Dicloxacillin sodium	Clonidine hydrochloride	LY 171883
Procaine hydrochloride	Clofazimine	Ibuprofen
Griseofulvin	Levetiracetam	Zacopride hydrochloride hydrate
Mexiletine hydrochloride	Isoquercitrin	Diphenylcyclopropenone
Fluocinolone acetonide 21-acetate	D-Cycloserine	Anastrozole
Fenofibrate	Alprazolam	Pirenperone
Symmetrel	Pantoprazole sodium	Stanozolol

Table A. Continued

Acetazolamide	Zafirlukast	Felbamate
(+/-)-Norepinephrine hydrochloride	Pidotimod	Verapamil hydrochloride
Flumadine hydrochloride	Ezetimibe	Rolitetracycline
Amitriptyline hydrochloride	AM-251	3-Pyridinemethanol
Phentolamine mono-hydrochloride	Fenpiverinium bromide	3'-Deoxydenosine
Cefotaxime sodium	Flurbiprofen	Procysteine
Desipramine hydrochloride	Exemestane	Doxylamine succinate
Etodolac	Orlistat	Etoposide
Clozapine	Medroxyprogesterone	Zonisamide
Tetrahydrozoline hydrochloride	Rizatriptan benzoate	Balsalazide
Allopurinol	Icariin	Digoxin
Busulfan	Alfuzosin	Racecadotril
Nateglinide	Finasteride	Piroxicam
Podofilox	2-Pyridylethylamine	Fluphenazine dihydrochloride
Hydroflumethiazide	Topiramate	RU-486
3,5,3'-Triiodothyronine	Vinorelbine tartrate	Deferiprone
Zidovudine	Nimodipine	Lomerizine dihydrochloride
Chlorzoxazone	HTMT dimaleate	Pinacidil monohydrate
Acebutolol hydrochloride	Dihydrexidine hydrochloride	Methylperone hydrochloride
Propantheline bromide	Ethylestrenol	Diazoxide
Ipriflavone	Temozolomide	Lobeline hydrochloride
Trihexyphenidyl hydrochloride	Zaleplon	Oxaprozin
Ru 24969 hemisuccinate	Risperidone	Gabexate mesilate
Flucytosine	Carisoprodol	Nimetazepam
Mepivacaine hydrochloride	Ranitidine hydrochloride	Primaquine diphosphate
Carvedilol	Fluocinolone acetonide	Amcinonide
Naltrexone hydrochloride	Methyldopa	Chlorpropamide
Cefuroxime	Theophylline	Mefenamic acid
Acetylcholine chloride	Hydrocortisone hemisuccinate	Flutamide
Lincomycin hydrochloride	Triamterene	Tolbutamide

Table A. Continued

Stavudine	Molindone hydrochloride	Doxapram hydrochloride
Propylthiouracil	Clobetasol propionate	Tizanidine hydrochloride
Econazole nitrate	Procainamide hydrochloride	Loteprednol etabonate
Pyrimethamine	Racepinephrine	Cefoxitin sodium
Ethambutol	Triclosan	Cortisone acetate
Amoxicillin	Mepenzolate bromide	Methimazole
Primidone	Amoxapine	Prednisolone acetate
Toremifene citrate	Sulindac	Mesalamine
Pralidoxime chloride	Hydrocortisone 17-valerate	Saquinavir mesylate
Chlorthalidone	Mebendazole	Midazolam hydrochloride
Glipizide	Atenolol	Fluvastatin
Mercaptopurine	Dopamine hydrochloride	Danazol
Duvadilan	Metaproterenol	Mitoxantrone hydrochloride
Isoniazid	Methoxsalen	Glyburide
Albendazole	Metoclopramide hydrochloride	trans-Retinoic acid
Terazosin	Thalidomide	Sulfinpyrazone
Cromolyn sodium	Disopyramide phosphate	Rifampicin
Oxytetracycline hydrochloride	Brimonidine	Vidarabine
Ribavirin	Nicotinic acid	Mefloquine hydrochloride
Sulfasalazine	Bendrofluazide	Mesoridazine besylate
Diphenhydramine hydrochloride	Zileuton	Trimethoprim
Sulfamethoxazole	Sotalol hydrochloride	Simvastatin
Kitasamycin		

APPENDIX B

Table B. Candidate Drugs Identified in Screen Against JCPyV

Drug Name	Function
Nicardipine hydrochloride	Coronary and cerebral vasodilator
Loperamide hydrochloride	Mu opioid receptor agonist
Pindolol	Beta-adrenoceptor blocker
Triamcinolone acetonide	Synthetic glucocorticoid steroid
Cetirizine	Antagonist of histamine (H1) receptor (second generartion)
Oxacillin sodium	Beta-lactam antibiotic
Lomifylline	Data limited (potential vasodilator)
Secoisolariciresinol	Plant based polyphenol of unknown mechanism
Benzylimidazole	May prevent DNA/RNA synthesis
Dantrolene sodium	Muscle relaxor- targets RyR1 and prevents calcium release
Isoniazid	Antituberculosis agent
Moclobemide	Reversible inhibitor of monoamine oxidase A
Omeprazole	Hydrogen/Potassium ATPase inhibitor
CCPA	Specific receptor agonist for the adenosine A1 receptor
Naftopidil	α1A-adrenoceptor antogonist
CGS 12066B dimaleate	Selective serotonin 1B receptor agonist
Milrinone	PDE3 inhibitor
Telmisartan	Angiotensin II receptor blocker
Ramipril	Angiotensin converting enzyme (ACE) inhibitor
Ampiroxicam	Prostaglandin-endoperoxide synthase inhibitor (NSAID)
Xanthinol nicotinate	Vasodilator peripheral and cerebral
Levetiracetam	Targets SV2A at synapse (antiepileptic)
Isoquercitrin	Unknown mechanism (flavonoid)
Fenpiverinium bromide	Anticholinergic agent (limited data)
Flurbiprofen	Cyclooxygenase inhibitor (NSAID)
Exemestane	Aromatase inhibitor
Rizatriptan benzoate	Selective 5-hydroxytryptamine 1B/1D (5-HT1B/1D) receptor agonist
Topiramate	Calcium channel blocker (Antiepileptic)
Nimodipine	Calcium channel blocker (cerebral vasodilator)

Table B. Continued

HTMT dimaleate	Histamine (H1) receptor agonist
Danazol	Synthetic steroid (androgen), reduces estrogen production
Cimetidine	Antagonist of histamine (H2) receptor
Isradipine	Calcium channel blocker (coronary, peripheral, and cerebral vasodilator)
Pilocarpine hydrochloride	Cholinergic agonist (target muscarinic receptors)
Nicorandil	Potassium channel activators (prevents calcium buildup within cell)
Pergolide mesylate	Dopamine receptor agonist
Bifonazole	Imidazole
Nifedipine	Blocks Ca activated K channel
Trifluoperazine hydrochloride	Dopamine receptor blocker (antipsychotic), Inhibitor of calmodulin
Beta-estradiol	Activates estrogen receptor
Ranolazine dihydrochloride	Partial fatty acid oxidation (pFOX) inhibitor
Paroxetine maleate	Selective serotonin reuptake inhibitor

BIOGRAPHY OF THE AUTHOR

Mason Crocker was born in Portland, Maine in December 1993. He graduated from Gorham High School in 2012. He attended the University of Maine and graduated in 2018 with a Bachelor's of Science degree in Microbiology. He entered in the Molecular and Biomedical Sciences graduate program at The University of Maine in Fall of 2018. Mason is a candidate for the Master of Science degree in Microbiology from the University of Maine in May 2020.